The Biochemical Characterization of VC0430: A Glutamate and Glutamine Binding SBP from the Poorly Understood Secondary Active Transporter TAXI-TRAP Family Found in *Vibrio cholerae.*

Joseph Davies

Kent ID: 17884666

Thesis Submitted to the School of Biosciences, University of Kent

MSC-R in Biochemistry

2022

Supervisor: Dr Chris Mulligan

Word Count: 15,375

Declaration

No part of this thesis has been submitted in support of an application for any degree or qualification of the University of Kent or any other University or Institute of learning.

Signature: Joseph Davies

Date: September 2022

Acknowledgements

Thanks for the support of Dr Chris Mulligan for his help and guidance throughout the year. I also want to thank Dr Andrew Daab and Tom Paige for their expertise and knowledge in protein crystallography as they have helped me tremendously.

Abstract:

The import of solutes into the bacterial cytoplasm involves many different membrane transporter types with some being active transport systems. Of these active transporters exist a group of secondary active transporters that require an SBP for substrate binding known as TAXI-TRAP transporters. To date, no biochemical characterisation of a TAXI-TRAP SBP exists in the literature. In *Vibrio cholerae,* VC0430 is an SBP from a TAXI-TRAP transporter that binds glutamate and glutamine *in vitro*.

In this study we biochemically characterize the TAXI-TRAP SBP VC0430 by determining the specificity and Kd for L-glutamate, D-glutamate, and L-glutamine by intrinsic tryptophan fluorescence. We then generated a homology model of VC0430 and mapped it against the only known structure of a TAXI-TRAP SBP, the glutamate/glutamine binding protein TTGluBp. From this structural alignment we were able to identify key binding site residues involved in substrate binding and mutated them to alanine to determine the key substrate selectivity determinants of VC0430. Furthermore, we also optimized crystallography conditions of VC0430 in the substrate bound and *apo* states for structural determination by X-ray diffraction.

We revealed that substrate binding in VC0430 is heavily dependent on specific hydrogen bonds with the amine group of glutamate/glutamine and specific non-polar interactions with two aromatic residues in the binding site. We further speculated on the role of glutamate/glutamine in the survival of the bacteria in its environment. Particularly in the role of glutamate is a precursor for a compatible solute that is required for survival in a high saline environment, highlighting VC0430 as a potential drug target.

Abbreviations

ABC ATP Binding Cassette

Amp Ampicillin

Apo Ligand Free Protein

a.u Arbitrary Units

DTT Dithiothreitol

DSF Differential Scanning Fluorimetry

FT Flow Through

IMAC Immobilised Metal Affinity Chromatography

IPTG Isopropylthio-β-galactoside

Kan Kanamycin

Kd Dissociation Constant

LB Lysogeny Broth

MBP Maltose Binding Protein

Ni-NTA Nickel-chelating Nitrilotriacetic Acid

NBD Nucleotide binding domain

N.D. Not Determinable

OD_{600} Optical Density at 600nm

PMT Photon Multiplier Tubes

SBP Substrate Binding Protein

SDM Site-Directed Mutagenesis

SEC Size Exclusion Chromatography

SMDM Sodium Malonate Dibasic Monohydrate

SOC Super Optimal Broth with Catabolite Repression

TEV Tobacco Etch Virus

Tm Melting Temperature

TMD Transmembrane Domain

TPAT Tetratricopeptide Motif-Protein (TPR) Associated Transporter

TRAP Tripartite-ATP-independent Periplasmic

TTT Tripartite Tricarboxylate Transporter

W Wash

WT Wild Type

Contents

Chapter 1: Introduction

Background

Prokaryotes and Archaea use a wide variety of active transporter systems, defined by their different energetic coupling mechanisms(1). Within these, a large majority being secondary active transporters where substrate movement is coupled to an electrochemical movement or primary active transporters where substrate movement is directly coupled to ATP hydrolysis(1).Further within these Primary Active Transporters lies many different families of protein transporters with note of the ATP-binding cassette (ABC) transporter. Canonical ABC transporters are characterised by four functional domains: two nucleotide binding domains (NBDs) and two transmembrane domains (TMDs)(2). The NBDs facilitate ATP binding and hydrolysis while the TMDs facilitate the transport of the substrate into the cytoplasm via conformational changes(3). However, some ABC transporters use an additional substrate binding protein (SBP) which binds to the substrate and then interacts with the membrane component of the transporter as described by Neu and Heppel, 1965(4).

SBP dependent membrane transporters aid in the survival of many different prokaryotes in their respective environments by enabling a separate SBP to bind a required substrate with a very high affinity. Kd's of some SBPs have even been shown to be in the nano molar range such as SiaP with an estimated Kd 58nM in a study by Müller et al. (5). Due to this dependence of an SBP to bind substrate in these systems they make a valuable drug target for developing potential membrane transporter inhibitors(6).

Previously, SBPs had only thought to be involved in Primary Active Transporters such as ABC transporters, but more recently, SBP-dependent secondary active transporters have been characterised(7). Of these SBP-dependent secondary transporters two different major families exist: the Tripartite ATP-independent periplasmic (TRAP) transporters(7,8) and the tripartite tricarboxylate transporters (TTT)(9). Although these groups show very little sequence similarities they do share structural similarities in their "tripartite" nature of

containing three distinct peptides(10): a transmembrane helix protein (typically containing 12 subunits) thought to be involved in the movements of substrates into the cytoplasm, a 4-transmembrane helix protein with unknown function in TRAP transporters and a poorly conserved extramembrane SBP(9).

Despite a recent increase in knowledge of these secondary SBP-dependent transporters, considerably less is still known about them compared to the primary ABC transporters counterparts.

Despite the low sequence similarity between TTT and TRAP transporters, the SBPs share a similar bilobular "Venus Fly Trap" tertiary structure(11) comprised of a two wings made up by one beta sheet containing 4-6 strands, surrounded by alpha helices connected by a hinge(12). With no substrate bound (*apo* state) the two wings are open and upon substrate binding they close around the substrate in a very specific manner allowing the SBP to then interact with the transmembrane unit (Figure 1)(13). This model has been observed in TTT transporter systems but recent FRET-based studies on the well characterised TRAP transporter VcSiaP has alluded to a similar mechanism (11), suggesting that this mechanism is synonymous between TTT and TRAP transporter systems.

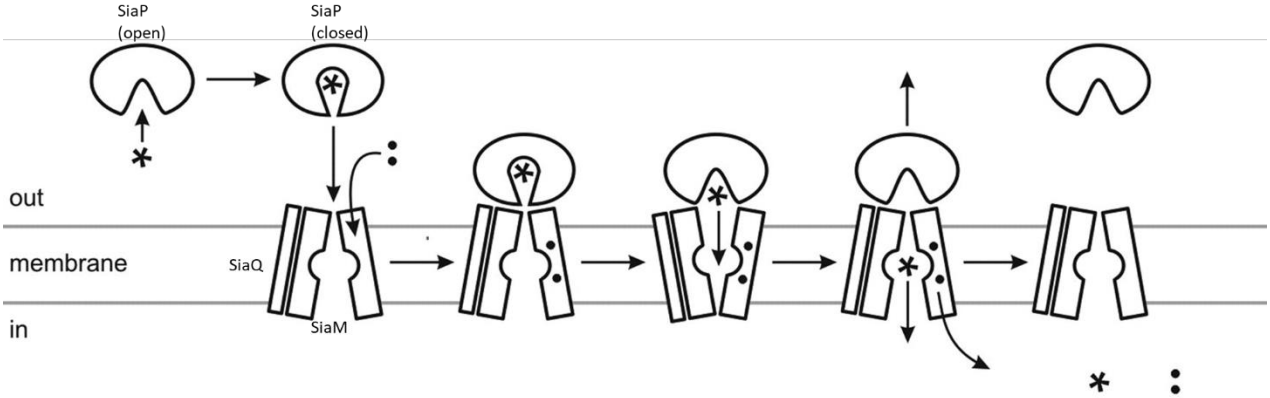

Figure 1 ***Model of substrate import by SiaPQM****. The SBP (SiaP) in the open conformation binds substrate (asterisk) and closes before binding to SiaQM coupled to the movement of Na+ ions (dots). SiaM then changes in conformation to the outward facing state to allow the substrate to enter before then changing conformation to the inward facing state to release the substrate and Na^+ ions into the cell. Figure adapted from Mulligan et al. (13).*

1.2. The TTT Family

Members of the TTT family are typically only found in bacteria and rarely found in archaea, unlike TRAP transporters(10). Of the two SBP dependent secondary active transporters that have been extensively characterised include the tricarboxylate transporter Tct of Salmonella typhimurium(14) and the dicarboxylate transporter Dct of Rhodobacter capsulatus(9), this Tct type is often cited as the founding member of the TTT

family. The TctABC transporter was characterised to contain three proteins; a large transmembrane protein with 12 predicted transmembrane components (TctA), a small transmembrane protein with 4 predictied transmembrane components (TctB) and a periplasmic SBP (TctC)(15). Although this TctABC shows a similarity in general architecture to the corresponding Dct type transporter (DctPQM) they bear very little sequence similarity and as such have been the foundation of two distinct families: the TTT group based on the TctABC transporter and the TRAP family based on the DctPQM transporter(9).

Currently, only a small number of TTT SBPs other than TctC have been biochemically characterised with only a limited number of structures available. Most of the current SBP structures come from B. pertussis and reveal a wide range of substrates other than tricarboxylates including the dicarboxylates aspartate, glutamate and nicotinate(16–18). Further studies have also shown how more TTT SBPs have an affinity for dicarboxylates in the nanomolar range for AdpC(10) and MatC(19) revealing a wider substrate range than initially anticipated.

1.3.1. The TRAP Family

The first TRAP transporter to be characterised was the high-affinity binding protein-dependent C4-dicarboxylate transporter, encoded by the gene dctPQM genes in *Rhodobacter capsualatus*(9). The TRAP transporter systems share similarities with the well documented ABC transporter family and the TTT family, with similar protein topology, composition and gene organization(12,15). TRAP transporters of the DctPQM family consist of three major subunits; a periplasmic SBP subunit (DctP) and two transmembrane subunits; a 12 transmembrane helices protein (DctM) and a 2 transmembrane helices protein (DctQ)(9,12). Although only a few examples of a complete TRAP transporter have been characterised(20), after a genome sequence analysis revealed a large variety of dctP gene homologues in prokaryotes but none in eukaryotes resulting in the crystallization of seven different SBPs from different organisms(21). The structure of these SBDs gives great insight into the SBDs of other TRAP transporters revealing a highly similar topology to ABC SBDs and ligand interactions with a highly

conserved arginine residue (Arg-174)(12,22). This Arg-147 is implicated as being a key residue in ligand binding for DctP-like SBPs but has also been speculated in having a wider role in the transport mechanism such as triggering domain closure(22).

Table 1 ***Crystallised TRAP SBPs from a variety of organisms.*** *The table shows the current structures of known TRAP SBPs up to 2010. In most cases, the protein was crystallized in complex with substrate revealing a wide range of different carboxylic acid substrates. Adapted from Fischer et al. (21).*

SBP	Source Organism	PDB code	Substrate	Reference
SiaP	*Haemophilus influenzae*	2CEX 3B50 2CEY	Neu5Ac2en Sialic acid -	(Müller et al., 2006)
TakP	*Rhodobacter sphaeroides*	2HZL 2HZK	Sodium Pyruvate Glycerol	(Gonin et al., 2007)
DctP7	*Bordetella pertussis*	2PFY	Pyroglutamate	(Rucktooa et al., 2007)
DctP6		2PFZ	Pyroglutamate	(Rucktooa et al., 2007)
TeaA	*Halomonas elongata*	2VPO 2VPN	Hydroxyectoine Ectoine	(Kuhlmann et al., 2008)
UehA	*Silicibacter pomeroyi*	3FXB	Ectoine	(Lecher et al., 2009)
TM0322	*Thermotoga maritima*	2HPG	ND	(Cuneo et al., 2008)
LakP	*Thermus thermophilus*	2ZZV 2ZZW 2ZZX	Calcium lactate Zinc lactate Lactic acid	(Akiyama et al., 2009)

However, to date, the best characterized TRAP transporter system is SiaPQM from H. influenza. SiaPQM was found to be essential for the uptake of sialic which is a key component of lipopolysaccharide which is known to play a role in bacterial resistance against human serum(23). Furthermore, SiaPQM remains the only TRAP transporter system to be reconstituted, revealing how transport required the presence of the SBP (SiaP) and sodium ions, suggesting that transport is powered by a sodium gradient(13).

Subsequent studies on TRAP transporters have revealed a wide variety of SBP based TRAP transporters in a wide variety of organisms, with most of the work being done on the extracytoplasmic SBP component(7,8). Based on these SBPs three distinct types of TRAP transporters have been identified; The classical DctPQM type as described the TAXI-TRAP group and the tetratricopeptide motif-protein (TPR) associated transporter (TPAT) group.

1.3.2 The TAXI-TRAP Subfamily

Unlike the classical TRAP transporters, the TRAP associated extrocytoplasmic immunogenic (TAXI) TRAP transporters, named after an immunogenic protein in *Brucella abortus*(24), share very little sequence similarity to DctP, do not have the conserved Arg-147 residue and are the only TRAP transporter found in archea(7). The various SBP structures involved in these different proteins have been grouped into 6 distinct clusters: A to F with further sub-divisions within each cluster(25). Based on this classification system, the DctP-like-TRAP-SBPs form their own unique cluster (cluster E) while TAXI-TRAP-SBPs are identified in a different cluster (cluster F) and bear a closer resemblance to ABC Transporter SBPs for trigonal planar anions such as bicarbonate and nitrate(21), warranting the classification of their own subfamily of TRAP transporters. However, although TAXIs have limited sequence similarity they do share general structural similarities with the general architecture of the membrane component (DctQM) remaining the same with a small transmembrane section and a larger transmembrane section, but as opposed to being separate proteins they appear to be fused together in TAXI systems (Figure 2)(12).

Despite initially being discovered 20 years ago the TAXI-TRAP transporters still remain to be poorly understood with the complete biochemical characterisation of one of these TAXI-TRAP systems still absent from the literature. Despite the lack of knowledge on TAXI's, a previous study by Rabus et al. 1999(26) revealed similarities in TAXI proteins to *E. Coli* glutamate/glutamine binding proteins suggesting that TAXI-TRAP transporters are possibly key glutamate/glutamine transporters. This idea is further supported by the only known structure of a TAXI TRAP protein solved by Takeshi et al. 2004 in the archaea *Thermus thermophilus*(27) (TTGluBp), co-crystallized with bound substrate that is either L-glutamate or L-glutamine. However, later, a study Bakermans et al. revealed how in a dctT (the SBP component of a TAXI-TRAP transporter) knockout strain of *P. arcitus*, resulted in severely reduced growth on acetate, butyrate and fumarate enriched media(28) potentially revealing a wider substrate range than initially thought. Additionally, a TAXI-TRAP transporter in the denitrifying bacteria *Azoarcus* sp. CIB has been identified as a key importer of the aromatic compound o-pthalate for degradation which is one of the key constituents of plastics and plasticisers revealing a potential of TAXI-TRAP transporters in the biodegradation of plastics in the biotechnology industry(29).

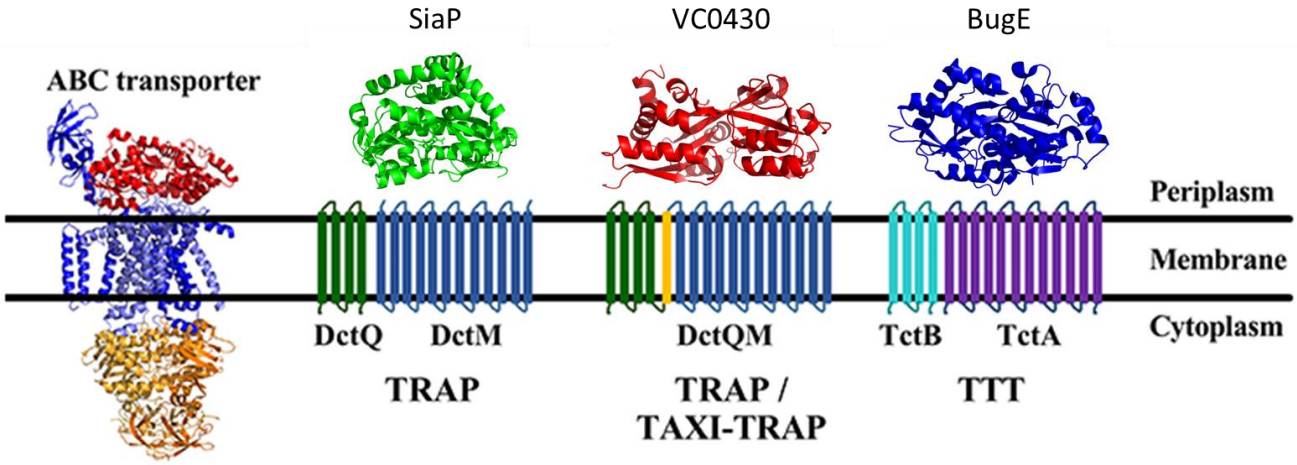

Figure 2 ***Schematic showing the three main classes of SBP-dependant Secondary Active Transporters****. SiaP as a TRAP transporter in green (PDB: 3B50), VC0430 as a TAXI-TRAP transporter in red with the fused membrane component and BugE as a TTT transporter in Blue (PDB: 2DVZ). All these transporter systems share a tripartite nature, with two transmembrane domains and periplasmic SBP.*

1.3.3. The TPAT Subfamily

As well as the TAXI subfamily of TRAP transporters, a study by Deka et al. on Treponema pallidum, the bacterial agent of syphilis, revealed a new subfamily known as tetratricopeptide motif-protein (TPR) associated transporter (TPAT)(30). In this case the genes encoding the TRAP components from T. pallidum, tp0957 (the SBP) and tp0958 (the membrane component) are present in an operon with a third uncharacterized gene(30). Crystallization of the SBP component Tp0956 also revealed how the SBP shares a similar two-lobe structure observed in traditional TRAP SBPs but further bioinformatic analysis showing how this whole transport system exemplifies a new subfamily of TRAP transporters(30). Protein analysis of this TPAT transporter reveals that it is a membrane complex comprised of four proteins with corresponding DctPQM architecture but an additional fourth protein with unknown function being referred to as the “T” component(31). Interestingly, this T component (TatT) exists as a trimer and has been crystallized in a complex with the SBP ($TatP_T$) in a way that

suggests substrate transfer between them takes place(31). The current hypothesis suggests that both TatT and $TatP_T$ remain tethered to the inner and outer membrane of T. pallidum and transfer the substrate from TatT in the outer membrane to $TatP_T$ in the inner membrane where the QM component is present to import the substrate into the cell(Figure 3)(31). The current substrate range of the TPAT system remains unknown but is possibly hydrophobic and different to other TRAPs due to a the highly hydrophobic makeup of the Tp0957 SBP(30).

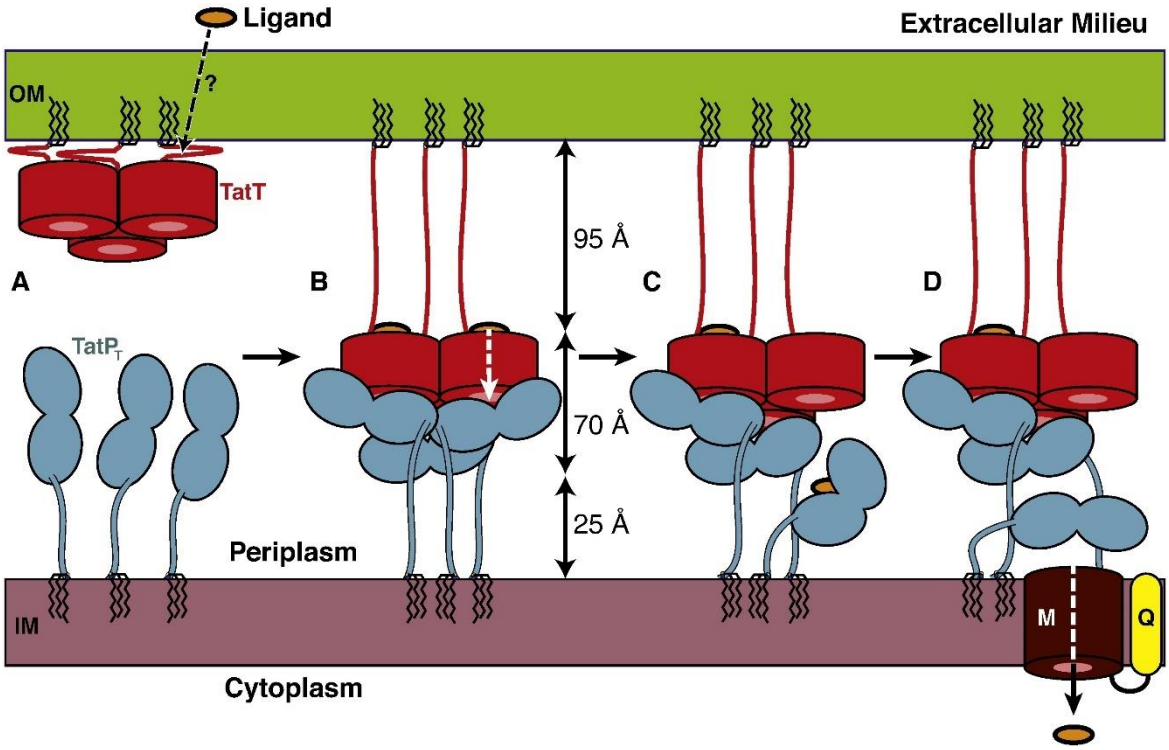

Figure 3 ***A current model of the proposed mechanism of TPAT transport****. (A) TatT (red) tethered to the outer membrane binds the ligand (orange) and transports it (B) across the periplasm to the SBPs ($TatP_T$, blue) tethered to the inner membrane where the ligand is transferred. (C) The ligand-$TatP_T$ complex then binds to the QM translocation apparatus to (D) import the ligand into the cytoplasm.*

1.4. Project Goals

The goal of this project on the TAXI-TRAP SBP, VC0430, was to expand the repertoire of biochemically characterised TAXI-TRAP SBP by:

- Determining an estimate of the Kd of the D and L enantiomers of its known substrates glutamate and glutamine
- Characterizing the binding site by screening residues for selectivity determinants of glutamate and glutamine by site directed mutagenesis

- Generating protein crystals of VC0430 in the apo, L-glutamate bound, and L-glutamine bound states for structural determination

Chapter 2: Methods and Materials

2.1. Strains, Plasmids, Media, and Buffers

2.1.1. Strains of *E. Coli* used

Table 2 ***A list of all E. Coli strains used in this project****.*

Strains of *E. Coli*	**Source**	**Genotype**
BL21(DE3)	Robinson Lab, University of Kent	F–ompT hsdSB (rB–, mB–) gal dcm (DE3)
NEB-5α	New England BioLabs	fhuA2Δ(argF-lacZ)U169 phoA glnV44 Φ80Δ(lacZ)M15 gyrA96 recA1 relA1 endA1 thi-1 hsdR17

2.1.2 Plasmids

Table 3 ***Plasmids used in this project****.*

Plasmid	**Protein**	**Antibiotic Resistance**
pRK793 (RRID:Addgene_8827)	Tobacco Etch Virus (TEV) Protease	Ampicillin
pEThisVC0430WT	VC0430	Kanamycin

2.1.3. Media

Table 4 ***A list of all cell media used.***

Media	**Composition**
Lysogeny Broth (LB)	For 1 L: 10 g NaCl, 10 g tryptone, 5 g yeast extract- added to MilliQ water and sterilised by autoclaving
LB Agar	For 1 L: 10 g NaCl, 10 g tryptone, 5 g yeast extract, 15 g agar- added to MilliQ water and sterilised by autoclaving
Super optimal broth with catabolite repression (SOC)	2 % vegetable peptone, 0.5 % yeast extract, 10 mM NaCl, 2.5 mM KCl, 10 mM $MgCl_2$, 10 mM $MgSO_4$, 20 mM Glucose. Used from NEB (Catalog number: #B9020).

2.1.4. Solutions and Buffers

2.1.4.1. Protein Extraction and Purification Buffers

Table 5 ***Buffers used in extraction and purification of TEV Protease by Ni IMAC chromatography***

Buffer	Composition
TEV Lysis Buffer	20 mM Tris pH 7.4, 300 mM NaCl, 10 % glycerol
TEV Purification Buffer	20 mM Tris pH 7.4, 300 mM NaCl, 20 % glycerol
TEV Wash Buffer	Purification buffer with 50 mM imidazole
TEV Elution Buffer	Purification buffer with 250 mM imidazole
Dialysis Buffer	20 mM Tris pH 7.4, 300 mM NaCl, 5 mM DTT, 5 % glycerol

Table 6 ***Buffers used in extraction and purification of VC0430 by Ni IMAC chromatography.***

Buffer	**Composition**
VC0430 Lysis Buffer	50 mM Tris pH 8, 200 mM NaCl, 5 % glycerol
VC0430 Wash Buffer	Lysis buffer with 20 mM imidazole
VC0430 Elution Buffer	Lysis buffer with 300 mM imidazole

Table 7 ***A list of different GHCl-containing wash buffers****. In order to unfold and refold VC0430 during the Ni-NTA purification, the column is washed with various concentrations of GHCl to unfold VC0430 and gradually refold VC0430 to remove any bound substrate.*

Standard Composition	**[GHCl] (M)**	**Total Resin Column Volumes**
50 mM Tris pH 8 200 mM NaCl 5 % Glycerol 20 mM Imidazole	2.0	30
	1.5	4
	1.0	4
	0.5	4
	0.0	8

All protein extraction and purification buffers were made up in MilliQ H_2O.

2.1.4.2. General Solutions and Buffers

Table 8 ***A summary of the main buffers used in this report****.*

Solution/Buffer		Compostion
SDS Gel Components	SDS PAGE Gel	Resolving: 6.9 mL 30 % Bis-acrylamide 37.5:1, 2.6 mL 1.875 M Tris pH 8.8, 130 µL 10 % SDS, 3.77 mL dH_2O, 130 µL 10 % Ammonium Persulphate (APS) and 13 µL Tetramethyl ethylenediamine (TEMED) Stacking: 1.69 mL 30 % Bis-acrylamide 37.5:1, 1.625 mL 1M Tris pH 6.8, 130 µL 10 % SDS, 9.56 mL dH_2O, 130 µL 10 % APS and 13 µL TEMED
	10X Running Buffer	30 g Tris, 150 g Glycine, 10 g SDS-Made up to 1 L with MilliQ H_2O
	4X SDS Sample Running Buffer	12 g Glycerol, 10 mL 10% SDS, 1 mL 1 M Tris pH 7.2, 0.06 g Bromphenol Blue and 3 mL MilliQ H_2O
	Coomassie Brilliant Blue Dye	50 % Methanol, 50 % Acetic acid and 0.2 % Coomassie Blue
	Coomassie Destain	20 % Methanol and 10 % Acetic acid – made up to volume with MilliQ H_2O
Assay Buffers	Differential Scanning Fluorimetry (DSF) Buffer	50 mM Tris pH 8, 20 mM NaCl
	Intrinsic Tryptophan Fluorescence Buffer	50 mM Tris pH 7.4
SEC Buffer	Size Exclusion Chromatography (SEC) Buffer	VC0430 Lysis Buffer (degassed)
Antibiotics	Kanamycin (Kan)	In all media it was used in it was used at a working concentration of 50 µg/mL
	Ampicillin (Amp)	In all media it was used in it was used at a working concentration of 100 µg/mL

2.2. Molecular Biology Techniques

2.2.1. DNA Miniprep

All minipreps were done with the QIAprep kit from Qiagen to purify plasmid DNA. First, 5 mL of LB with either Kanamycin or Ampicillin at 50 µg/mL and 100 µg/mL respectively was inoculated with cells from a glycerol stock stored at -80°C via scraping with a pipette tip. The inoculated LB was then grown overnight at 190 rpm, 37°C (standard conditions). The next day the cells were harvested by centrifugation at 13000xg

for 3 minutes at room temperature. The plasmid was then extracted as per the instructions on the kit, except only 30 µL of elution buffer was used and the elution buffer was left for 10 minutes on the column before eluting. The DNA absorbance at 260nm was then measured with a nanodrop to determine the concentration before being stored in a freezer at -20°C.

2.2.2. Transformations

In sterile conditions, *E. coli* of the desired strain (from glycerol stocks) were used to inoculate 5 mL of LB and left overnight under standard conditions. The next day, 0.5 mL of the overnight culture was then added to 4.5 mL of fresh LB and left for 2 hours under standard conditions to refresh the cells. Next, the refreshed cells were split into 1 mL aliquots in sterile Eppendorf's and then harvested by centrifugation at 13000xg for one minute at room temperature. The harvested cells were resuspended in 50 µL of ice cold 100 mM $CaCl_2$, creating multiple 50 µL shots of chemically competent cells that were left on ice until needed.

2.2.2.1. Transformation by Heat-Shock

100 ng of plasmid DNA was mixed into a single 50 µL shot of chemically competent BL21(DE3) cells for expression or a premade shot of ultra-competent cells (NEB-5α), that had been thawed on ice for 10 minutes, the cells with the plasmid was then left on ice for 30 minutes. After this incubation, the cell mixtures were heated for exactly 45 seconds at 42°C in a dry heating block and moved back on to ice for 5 minutes. Following this, 200 µL of SOC was added to the cell mixture and moved to an incubator at standard conditions for 1 hour. Next, approximately 50 µL of the transformant mixture was added to a selective LB plate of required antibiotic to incubate overnight at 37°C. Colonies on the plates were observed and counted the next day.

2.3. Expression of TEV Protease

150 mL LB with Ampicillin (LB_{Amp}) in a 500 mL conical flask was inoculated with transformed BL21(DE3) containing the TEV plasmid from a glycerol stock stored at -80°C and then grown overnight under standard conditions. The following day, six 5 L conical flasks containing 1L of LB_{Amp} was inoculated with 20 mL each of the overnight culture and grown under standard conditions. Growth was monitored by the absorption of light at 600 nM (OD_{600}) in a 1 mL cuvette using a spectrophotometer. Once the OD_{600} had reached 0.5-0.6 it was induced with 0.4 mM isopropylthio-β-galactoside (IPTG) and left overnight under standard conditions. The next day, the cells were harvested by centrifugation at 4000 xg for 20 minutes at 4°C and then resuspended and homogenised in TEV lysis buffer (Table 5), 15 mL per 1 L of culture. After this, the cell suspension was lysed by a cell disrupter with 3 passes at a pressure between 10,000-20,000 psi in the mini cell. The following cell lysate was then centrifuged at 20,000 xg for 20 minutes at 4°C and the supernatant (clarified lysate) was then collected for purification.

2.4. Purification of TEV Protease

To purify the TEV clarified lysate Immobilised Metal Chromatography (IMAC) Nickel-chelating nitrilotriacetic acid (Ni-NTA) resin (Qiagen) in a 4°C cold room in a two-stage process. 1 mL (0.5 column volumes, CV) of washed and equilibrated Ni-NTA resin per 1 L of culture was added to the clarified lysate and agitated for 30 minutes at 4°C. The resulting mixture was then added to one or multiple 25 mL purification columns to allow the flowthrough to be collected. The column was washed with 20 CV of TEV wash buffer (Table 5) before eluting the TEV in one elution step with 10 CV of TEV elution buffer (Table 5). Next, to remove the imidazole as it inhibits TEV, the eluted TEV was then dialysed in dialysis tubing with an 8 kDa molecular weight cut off (Biodesign D102) in 4 L of dialysis buffer (Table 5) overnight at 4° C. For the second stage, the TEV was re-incubated with the same resin and purified again as described. The now pure TEV had the absorbance at 280 nm (A280) read with a nanodrop to estimate concentration in mg/mL before being stored at -20°C until needed.

2.5. Expression of VC0430

After transforming competent *E. Coli* (BL21(DE3)) with the desired plasmids, multiple colonies were picked with a pipette tip and put into 50 mL LB with Kanamycin (LB_{Kan}) in a 250 mL conical flask that was then incubated overnight at standard conditions. The next day, 10 mL of the overnight culture was used to inoculate 1 L of LB_{Kan} in a 2.5L Tunair flask under standard conditions. The OD_{600} was monitored with a spectrophotometer in 1 mL cuvettes, once the OD_{600} had reached between 0.6-0.8 the culture was induced with 1 mM IPTG and left overnight under standard conditions. The following day the cells were harvested by centrifugation at 4000xg for 20 minutes at 4°C. The pelleted cells were then resuspended and homogenised with 50 mL VC0430 lysis buffer (Table 6) per 1 L of culture. To lyse the cells the resuspended cell suspensions were put through a cell disrupter 3 times at a pressure of between 10,000-20,000 psi in the mini cell. Next, the cell lysate was clarified by centrifugation at 20,000 xg for 20 minutes at 4°C, the supernatant was then collected and transferred to a new tube ready for purification.

2.6. Purification of VC0430

2.6.1 Nickel Affinity Chromatography

To purify the clarified lysate supernatant, IMAC was again used with (Ni-NTA) resin (Qiagen) at room temperature.

A 25 mL purification column was prepped with 1 mL of Ni-NTA resin (0.5 mL column volume, CV) per 1 L of initial cell culture, and left to rest for 2 minutes to allow the ethanol storage solution to flow through. The resin was then washed with 5 CV MilliQ H_2O and then equilibrated with 5 CV of VC0430 lysis buffer (Table 6). 25 mL of clarified lysate supernatant was then added to the column and the flow through was collected. The column was then proceeded to be washed in five steps with wash buffer containing varying concentrations of GHCl (Table 6 and 7) to unfold and refold the protein to remove bound substrate. Finally, the bound VC0430 was then eluted in 5 elution steps (E1-5) with 0.5 CV of elution buffer (Table 6) for E1 and 2 CV of elution buffer for E2-5. To assess the quantity of VC0430 in E1-5 the A280 was read on the nanodrop to get an estimate of the concentration in mg/mL.

2.6.2 HIS Tag Removal by Digestion with (Tobacco Etch Virus) TEV Protease

To effectively perform Intrinsic Tryptophan Fluorescence (ITF) it was deemed necessary to remove the large 6.5 KDa His-Flag tag from VC0430. To do this E1-5 were collected and recombined in dialysis tubing with an 8 kDa molecular weight cut off (Biodesign D102) in 4 L of dialysis buffer (Table 5) and dialysed overnight at 4°C. The following day the dialysed VC0430 was removed from the dialysis tubing and incubated with approximately half the volume TEV Protease at 2 mg/mL for 3-4 hours at room temperature agitating. After this incubation the VC0430-TEV mixture was added to a 25 mL column containing Ni-NTA resin, prepared as before. Once the VC0430-TEV mixture was added to the column the column was then mixed for 30 mins at 4°C to make sure that all the TEV can bind to the column. Next, the flowthrough from the column (FT2) was collected as it should contain VC0430 without the HIS tag because it should no longer bind to the NI-NTA resin.

2.6.3 Size Exclusion Chromatography (SEC)

Size Exclusion Chromatography (SEC) of the cleaved VC0430 FT2 was performed using a 24 mL Superdex 200 Increase 10/300 GL column at a 0.5 mL min^{-1} flow rate in an AKTA purification system. Before being administered into the AKTA for SEC the VC0430 FT2 was concentrated to 1 mL by Pierce™ Protein Concentrator PES, 2-6 mL with a 10000 Da Molecular Weight Cut off from ThermoFisher (catalogue: 88517) by centrifugation. After, the concentrated protein was ultra-centrifuged at 60,000 rpm at 4°C and the supernatant was put on to the AKTA that had been washed with degassed MilliQ H_2O and equilibrated with degassed VC0430 lysis buffer. The fractions of the SEC purified protein were then collected, used for SDS PAGE and then aliquoted out and snap frozen at -80°C in a dry ice ethanol bath for long term storage.

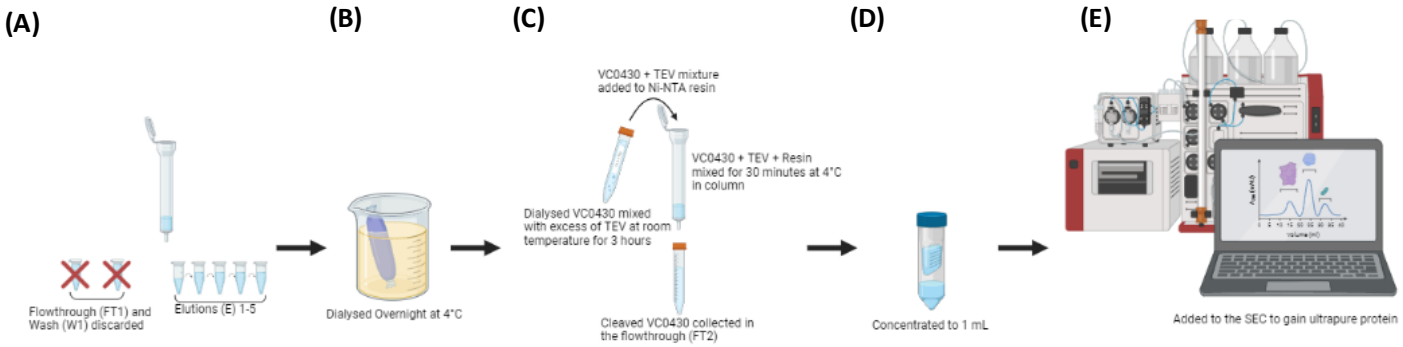

Figure 4 ***Schematic for the entire purification process and HIS-Tag removal with TEV****. First, VC0430 is purified from clarified lysate and 5 elutions are collected. The elutions are then dialysed overnight (B). Next, an excess of TEV was added to the dialysed VC0430 to mix for 3 hours at room temperature before being added to Ni-NTA resin in a column and mixed for another 30 minutes at 4°C. The following flowthrough was then collected (FT2) which should be VC0430 without the HIS-tag (C). After, the cleaved VC0430 was then concentrated to a volume of 1 mL (D) and ultracentrifuged at 60,000 xg at 4°C (not shown). Finally, the supernatant was added to the AKTA for ultrapure protein (E).*

2.7. Differential Scanning Fluorimetry Binding Assay

The Differential Scanning Fluorimetry (DSF) Binding Assay was performed as describes by Vedadi et al. (32), with slight variation for VC0430. All the assays were completed in a QuantStudio 3 RT-PCR machine and experimental design was done with QuantStudio Design and Analysis Software (ThermoFisher, Figure 5). The substrates for analysis were made up at a stock concentration of 50 mM in MilliQ H_2O and had the pH adjusted to as close to pH 7 as possible with KOH. The assay was done in triplicate 50 µL samples with 5 µM protein with varying concentrations of substrate from 1 mM to 15 mM and 2.5x SYPRO Orange Dye (MercK) made up in DSF buffer (Table 8). Samples were mixed in PCR tubes with a desk-top microcentrifuge for ~30 seconds before each run. Each run had a control with protein but no substrate for the first set of tubes to use as a baseline. Post-run data was then exported and plotted in Microsoft Excel.

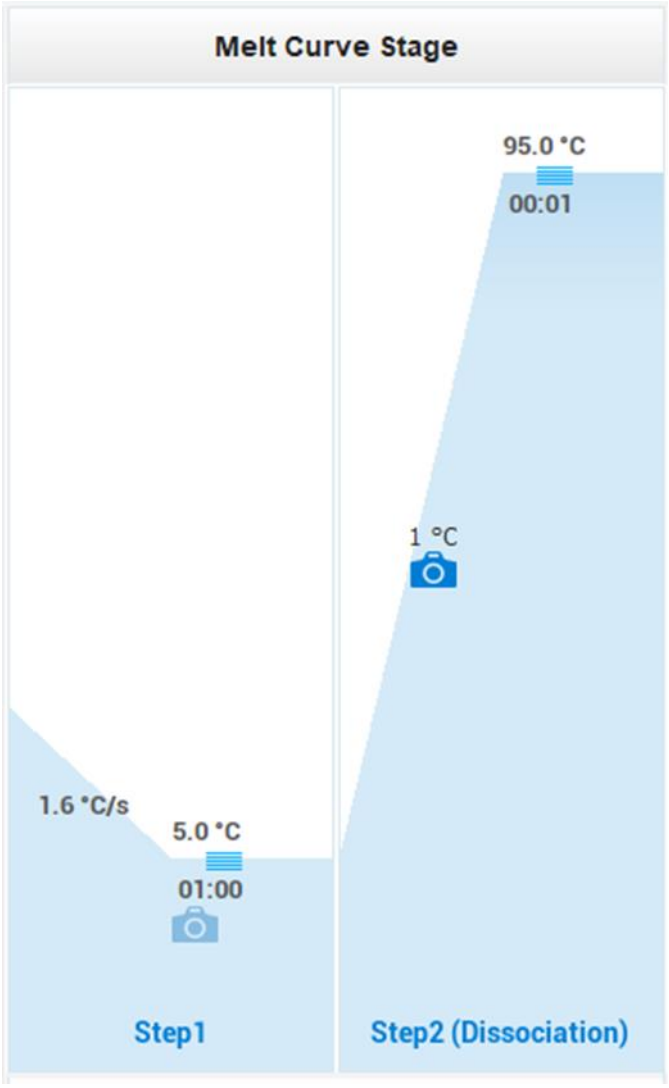

Figure 5 ***Schematic of the DSF experimental design****. Experimental design of DSF Binding Assay using QuantStudio Design and Analysis Software. Initially, the thermocycler temperature was cooled to 5°C at a rate of 1.6°C/s and then held for 1 minute, before gradually increasing by 1°C to a maximum of 95°C, taking a fluorescence reading at every increment. The reporter dye setting was set to SYBR and the passive reference was set to "ROX".*

2.8. Intrinsic Tryptophan Fluorescence

2.8.1 Intrinsic Tryptophan Fluorescence Initial Emission Scans

VC0430 contains two tryptophan residues Trp-96 and Trp-170, as such Intrinsic Tryptophan Fluorescence could take place. The fluorescence emission was measured using a Cary Eclipse fluorimeter (Agilent) in a 2 mL quartz cuvette. 0.5 µM of VC0430 was used in 2 mL of fluorescence buffer (Table 8). For all fluorescence an excitation wavelength of 295 nm was used and for the scans an emission range of 300 nm – 400 nm. To maximise a clean signal all the emission scans were done with an excitation and emission slit length of 10 nm with medium PMT voltage. Furthermore, to get a smoother signal to make observed

trends more discernible of the emission scan spectra, Savitzky-Golay smoothing of factor 15 was used (Figure 6). Different concentrations of substrate were added to the cuvette and mixed with a P1000 pipette to observe how it impacted the fluorescence signal. All fluorescence data was recorded at 20°C.

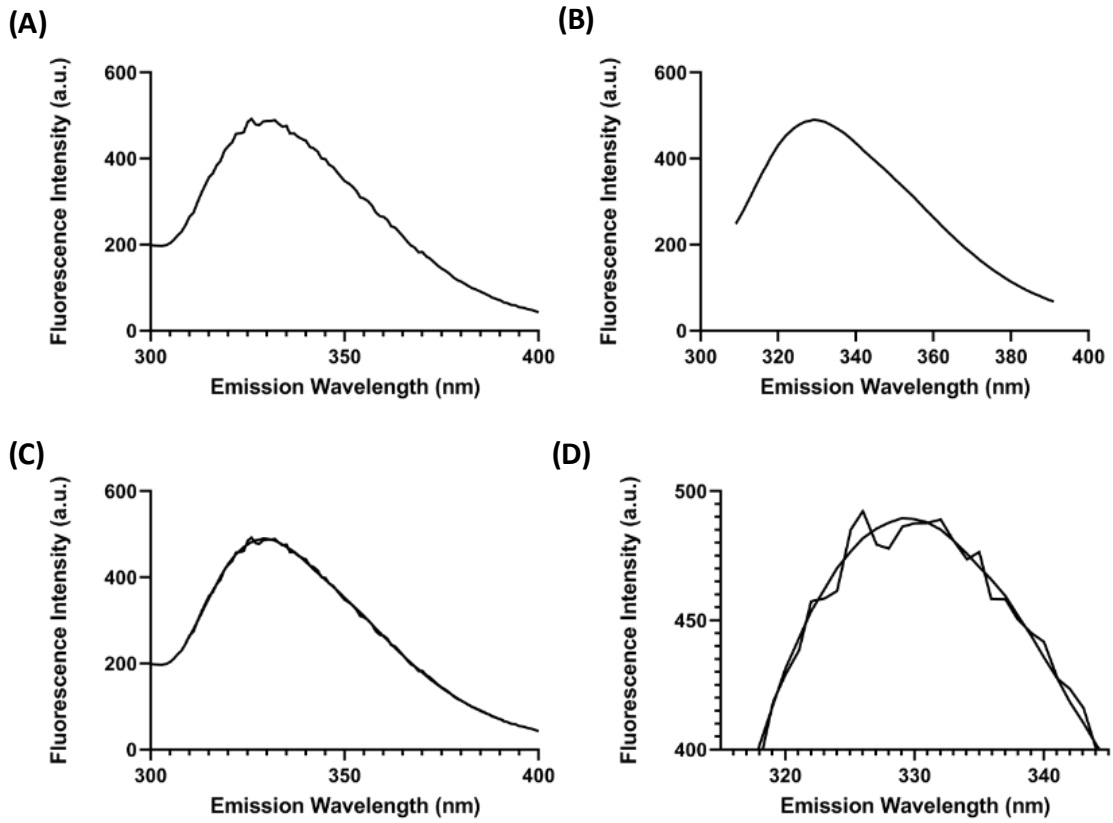

Figure 6 ***Smoothing optimisation of VC0430****. Emssion scan of VC0430 with no smoothing (A). Emission scan of VC0430 with Savitzky-Golay Smoothing factor 20 (B). Overlay of VC0430 emission scan with and without smoothing (C). Overlayed trace of the peak of the VC0430 emission scan with and without smoothing. Although the data is altered slightly the overall trend remains the same.*

2.8.2 Glutamate and Glutamine Titrations

Intrinsic Tryptophan Fluorescence was also used for titrations by adding increasing concentrations of substrate and reading the fluorescence signal to construct a binding curve to estimate the dissociation constant (Kd). We used different stock concentrations of ligand originating from a 50 mM stock, in such a way that no more than 2 µL of substrate was used in each addition making the effects of dilution negligible. For the titrations, unlike the emission scans the excitation wavelength was set to 295 nm but the emission wavelength was set to a constant 330 nm resulting in a plot of Fluorescence Signal Intensity (a.u) at 330 nm against Time (s). To try and minimise photobleaching but maximise signal the excitation slit was set to 5 nm and the emission slit to 10 nm. Initially, VC0430 had its fluorescence signal read for 30 seconds to establish a baseline and for each subsequent addition of

substrate after mixing with a P1000 pipette, the fluorescence signal was read for 20 seconds to further reduce the potential of photobleaching. After, the data was imported into Microsoft Excel where the average fluorescence signal for each cumulative concentration of substrate was calculated. To convert this to a binding curve the cumulative concentration of substrate was plotted against the change in fluorescence seen (Δfluorescence) as compared to the baseline reading with no substrate present. Once the raw data had been processed into a binding curve, the processed data was then imported to GraphPad Prism where it was fitted to the One Site Total Binding model by least squares fit to give an estimate of the Kd (Figure 7).

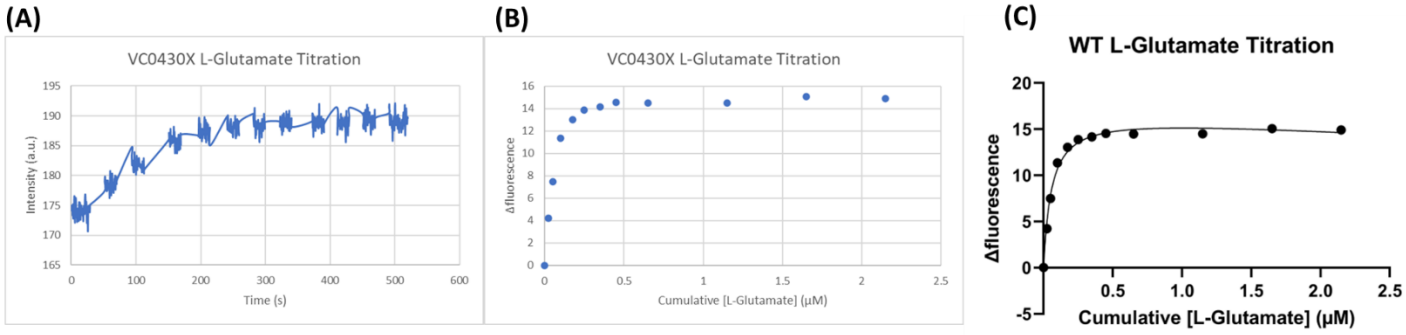

Figure 7 ***Construction and fitting of a substrate binding curve****. Raw data of a titration (A) each "block" is the fluorescence reading after a substrate addition. The change in average fluorescence signal plotted against cumulative substrate concentration (B). The average fluorescence of each substrate addition was calculated and the difference in average fluorescence from the no substrate baseline was plotted against the cumulative substrate concentration. The binding curve fitted to the One Site Total Binding model in GraphPad Prism to get an estimate of* K_D *(C).*

2.9. Homology Modelling and Binding Site Mapping of VC0430

No structure of VC0430 has been published yet, as such a predicted structure of VC0430 was generated by automated homology modelling with Phyre2. The closest match was an unnamed immunogenic protein from *Ehrlichia chaffeensis* (PDB ID: 4ddd) with 100 % confidence and a sequence identity of 41 %. However, another very good match was a periplasmic glutamate/glutamine-binding protein in *Thermus thermophilus* (PDB ID: 1us5, TtGluBp) with a 100 % confidence and a sequence identity of 38 %. Additionally, TtGluBp is one of the only known structures of a TAXI-TRAP transporter SBP that has been solved. Due to this structure being crystalized with glutamate bound it was compared to the predicted structure of VC0430 in PyMol to determine key binding residues for site-directed mutagenesis.

2.10. Site Directed Mutagenesis (SDM)

Primers were designed for mutagenesis of Tyr-45, Gln-93, Glu-125, Tyr-200 and Met-201 to alanine for VC0430 on the pEThisVC0430WT plasmid (Table 9). KOD Hot-start DNA-Polymerase from Sigma-Aldrich was used to generate the mutant plasmid in a 25 µL reaction volume with a composition as seen in Table 10. The reaction mixture was put in a BIORAD thermocycler, and the reaction proceeded under the conditions listed in Table 11. After SDM, the mixture was incubated with 2 µL Dpn1 for 2 hours at 37°C to remove the methylated template DNA. 2 µL of the mixture was then transformed into NEB-5α by heat-shock as described previously and transformed colonies were picked and grown overnight in LB_{KAN} to make a glycerol stock (400 µL 50 % glycerol, 600 µL culture) and be miniprepped. The pure plasmid from the miniprep was then sequenced by Eurofins LightRun Tube service. Plasmids confirmed to contain the desired mutation were then transformed into BL21(DE3) to be expressed and purified as done with Wild Type VC0430. Once, the mutants had been purified they were then used in DSF, and fluorescence as performed with Wild Type VC0430.

Table 9 ***VC0430 SDM primers****. Wild Type Sequence with relevant codon highlighted in green (Top) and primer designed with new alanine codon highlighted in yellow (Below).*

Forward Primer Sequence	Mutation
…GCCTTCATCTACATGGTTGGCCATCCAAATGGTGCC…	Y45A
GGTTCGGTTACTGGTGTTGCGTACCCTACGGGCGGC	
…GATTTCGGTATTGTGCAATCAGATTGGCAGTAC…	Q93A
GATTTCGGTATTGTGGCCTCAGATTGGCAGTAC	
…CTCAATGCACACCGAGCCTTTCAATATCATC…	E125A
CTCAATGCACACCGCGCCTTTCAATATCATC	
…GATGCCTTCATCTACATGGTTGGCCATCC…	Y200A
GATGCCTTCATCGCGATGGTTGGCCATCC	
…GCCTTCATCTACATGGTTGGCCATCCAAATGGTGCC…	M201A
GCCTTCATCTACGCCGTTGGCCATCCAAATGGTGCC	

*Table 10. **Reaction mixture for KOD polymerase SDM reaction***

Component	Final Concentration
10x KOD reaction buffer	1x
2mM dNTPs	200 µM
25mM MgSo4	1 µM
100 µM forward primer	5 µM
100 µM reverse primer	5 µM
10 ng/µl Template	0.2 ng/µL
KOD polymerase	0.02 U/l

*Table 11 **Thermocycler conditions for KOD SDM reaction**.*

Step	Temp	Time
Initial denaturation	98°C	30 s
25 cycles	98°C	10 s
	55°C	30 s
	72°C	40 s/kb
Final extension	72°C	2 min
Hold	10°C	FOREVER

2.11. Protein Crystallography

2.11.1. Hanging Drop Initial 96-Well Plate Screen

Two 96-well plates were prepared with 1.2 µL of precipitant solution of each condition of the JCSG+ (Molecular dimensions MD1-37) or Wizard Classic 3 & 4 (Molecular Dimensions MD15-W34-T). The 96-well plates were then taken to a mosquito where 200 nL of VC0430 at 15 mg/mL was added to adhesive ClearVue Sheets (Molecular dimensions MD6-01S) corresponding to each well before sealing the 96-well plate and leaving it in a 20°C temperature-controlled room. The plates were then left for two weeks before being checked for crystals with a microscope at 96x magnification.

2.11.2. Hanging Drop 24-Well Plate Optimisation

Promising solutions were then tested in 24-well plates, adding enough solution to cover the surface well (~500 µL). 2 µL of well solution was mixed with 2 µL of VC0430 at 15 mg/mL for a 1:1 ratio of protein to solution on a 22 mm cover slip. The ratio of protein to well solution was altered to find the optimum ratio. The cover slip was then sealed to the well with vacuum grease and left in a 20°C temperature-controlled room for one day before being checked. Other 24-well plates were also set up with VC0430 that had been incubated with 2 mM L-glutamine, 1 mM L-glutamine or 0.5 mM L-glutamate to crystallise VC0430 with substrate bound.

Chapter 3: Results

3.1. Expression and IMAC Purification of VC0430

Wild type VC0430 is a 35.255 kDa protein of 328 amino acids produced in *Vibrio cholerae* (Uniprot ID: Q9KU25). We used SignalP 5.0 to determine if VC0430 has a signal sequence, which predicted a signal sequence of the first 30 residues (2.977kDa) with a probability of 0.9425 (Figure 8), that does not directly contribute to the fold of VC0430, as such the signal sequence was removed in the plasmid that was used to produce VC0430 *in vitro*. We produced VC0430 in *E. coli* (BL21 (DE3)) with a pET plasmid vector containing a tag on the N-terminus of the protein consisting of a FLAG tag, a 10x His-tag and a TEV (Tobacco Etch Virus) protease cleavage site (Figure 9). This His tag consisted of 10 histidine residues at the N-Terminus with the total molecular weight of the tag being approximately 6.5 kDa which results in a total molecular weight of 35.872 kDa.

We then expressed the VC0430 plasmid in LB and purified the protein product with Ni-NTA affinity chromatography, eluting with imidazole in five different additions of elution buffer before then visualising the samples by SDS-PAGE (Figure 10). The SDS gel revealed bands that migrate to around the 35 KDa mark based on the ladder which corresponded with our estimation of 35.872 kDa that was predicted by the amino acid sequence. However, some contaminants were seen in the elution fractions on the gel but in significantly smaller relative intensity and size to the VC0430 bands. The high levels of protein seen in the elution's strongly suggests that it is VC0430 as it would be very unlikely for any other protein without a His-tag to bind to the Ni-NTA resin and be eluted in such large quantities.

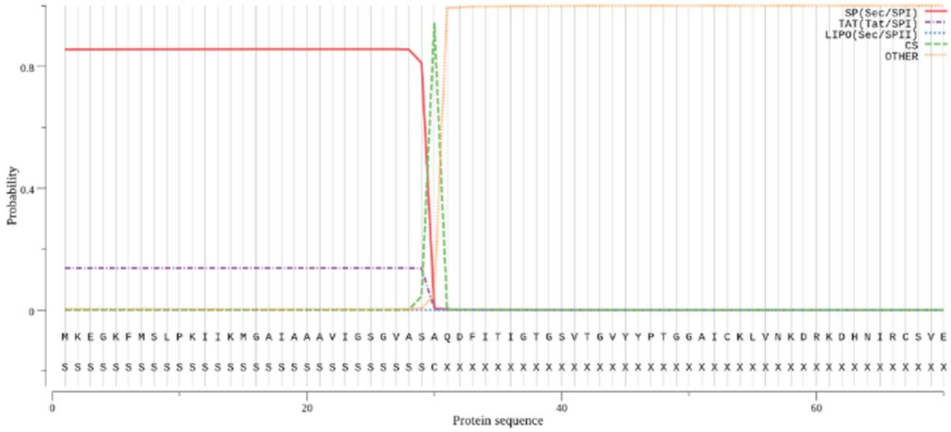

Figure 8 ***SignalP 5.0 analysis of the sequence of VC0430.*** *A screenshot of the SignalP analysis revealing a high probablity of a signal sequence up to residue 30 given by the green dashed line.(Nielsen & Krogh, 1998)*

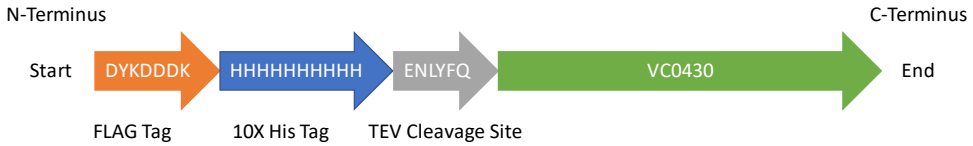

Figure 9 ***Schematic of VC0430 with the location of the tags and TEV Cleavage SIte in the Plasmid****. VC0430 (green) was produced with a FLAG tag of motif DYKDDK (orange) a 10X His tag (blue) and a TEV cleavage site of motif ENLYFQ (grey) at the N-terminus.*

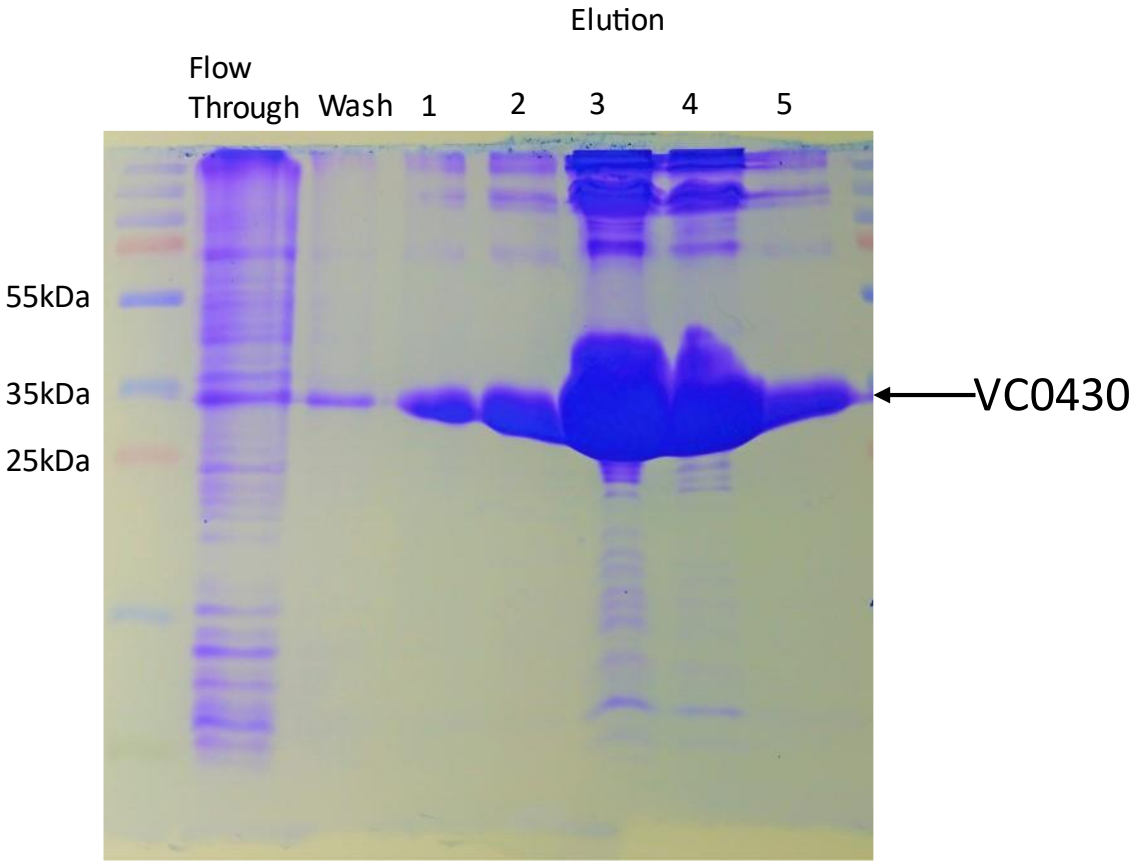

Figure 10 ***Production of VC0430****. SDS acrylamide gel stained with Coomassie Blue showing the Flowthrough (FT), Wash (W) and Elution's 1-5 (E1-5) of a VC0430 purification. VC0430 being seen close to the predicted molecular weight of 35.872KDa and indicated in the 5 elution's with an arrow.*

In future purifications of VC0430 for binding assays in the wash step we washed the resin with different concentrations of guanidine hydrochloride (GHCL) to unfold and refold the protein. Prior evidence strongly suggested that VC0430 binds glutamate and glutamine. These two compounds are abundant in *E. coli* (33)so to avoid a situation where the protein is purified with pre-bound ligand as has been seen for other SBPs(5), we denatured the

purified protein and refolded it. However, the binding assays we performed on refolded VC0430 gave identical results to the binding assays done without refolding VC0430, indicating that the protein was well folded.

3.2. Thermal Shift Assays of VC0430 Wild Type with D and L Glutamate and Glutamine

Differential Scanning Fluorimetry (DSF) is a quick, temperature-based assay that uses a small amount of protein and the SYPRO Orange dye, making it an ideal candidate for initial screening of substrate binding and specificity. The procedure works by using a fluorescent dye (SYPRO in our case) that binds to hydrophobic regions of a protein. As the temperature increases, the protein becomes more unfolded and therefore exposes more of these hydrophobic regions resulting in an increase in fluorescence signal (Figure 11A)(34). However, in our case instead of the fluorescence signal continuing to increase it was observed to decrease again. The derivative of this fluorescence signal can then be used to determine the melting temperature (Tm) by looking at the minimum fluorescence derivative reading (Figure 11B). If a substrate is bound the extra intermolecular interactions will result in a higher Tm when heated. Therefore, the bigger the difference in Tm (ΔTm) between protein with and protein without substrate the more likely it is that the substrate binds(34).

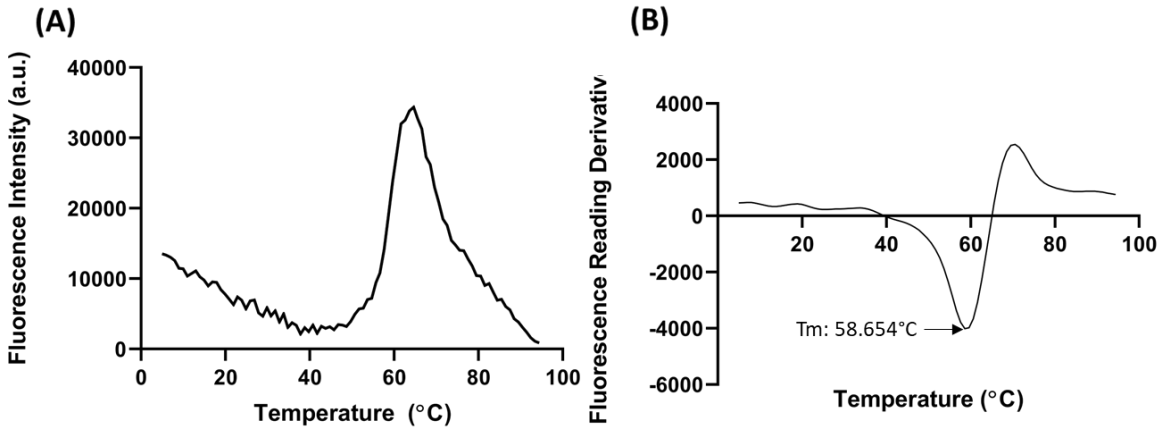

Figure 11 ***Melt Curve and Derivative Plot of VC0430****. Raw data melt curve plotting Fluorescence Intensity (a.u.) against Temperature (°C) (A) and derivative plot of fluorescence Reading Derivative against Temperature (°C) (B) of VC0430 with the Tm marked. Repeated 3 times.*

3.2.2. Assessing the Substrate Binding of VC0430 for L-Glutamate and L-Glutamine by DSF

Previous data suggested that VC0430 binds both L-glutamate and L-glutamine (C. Mulligan, personal communication). To confirm this, we performed DSF with purified VC0430 and incubated with 1 mM of L-glutamate

or L-glutamine to see if a significant ΔTm would be observed. We also used a triplicate of VC0430 with no substrate in each experiment to be used as a baseline. For both L-glutamate and L-glutamine, the Tm had increased significantly in both cases, indicating that they both bind to VC0430 (Figure 12). Furthermore, the change in melting temperature (ΔTm) upon addition of L-glutamate is much higher than what was seen for L-glutamine, suggesting that VC0430 may have a higher affinity for L-glutamate as it would potentially be able to form more noncovalent interactions with VC0430 than L-glutamine. Additionally, we tested two similar C4 Dicarboxylates to glutamate and glutamine, malate, and aspartate to probe the range of compounds VC0430 can bind and how selective it is. However, neither of them resulted in a significant increase in Tm (Figure 13), strongly suggesting that VC0430 does not bind them and is highly selective.

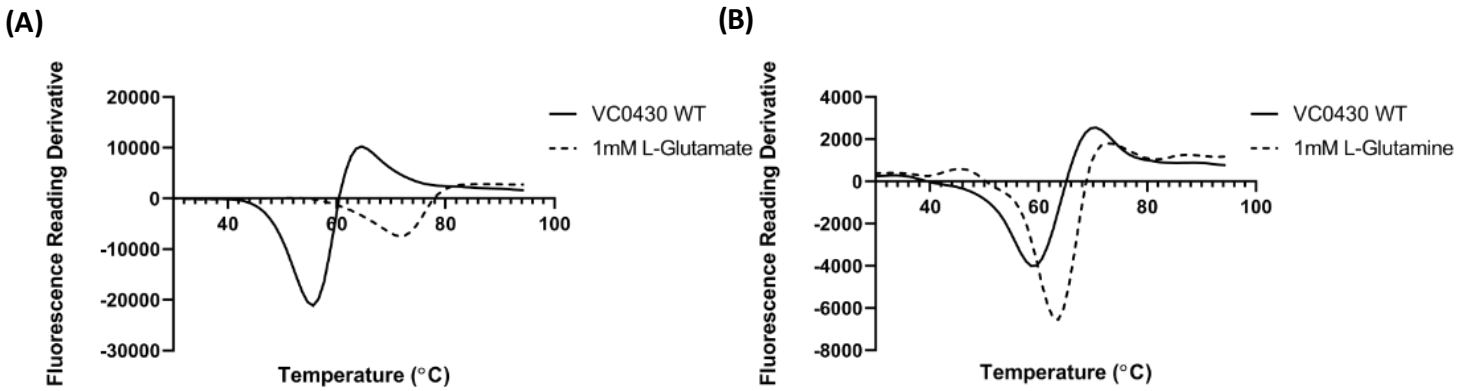

Figure 13 ***VC0430 L-glutamate and L-glutamine derivative plot.*** *Derivative Plot of VC0430 with 1 mM L-glutamate, VC0430 with no substrate as the solid line and VC0430 in the presence of 1 mM L-glutamate as the dashed line (A). Derivative Plot of VC0430 with 1 mM L-glutamine, VC0430 with no substrate as the solid line and VC0430 in the presence of 1 mM L-glutamine as the dashed line (B). Repeated 3 times.*

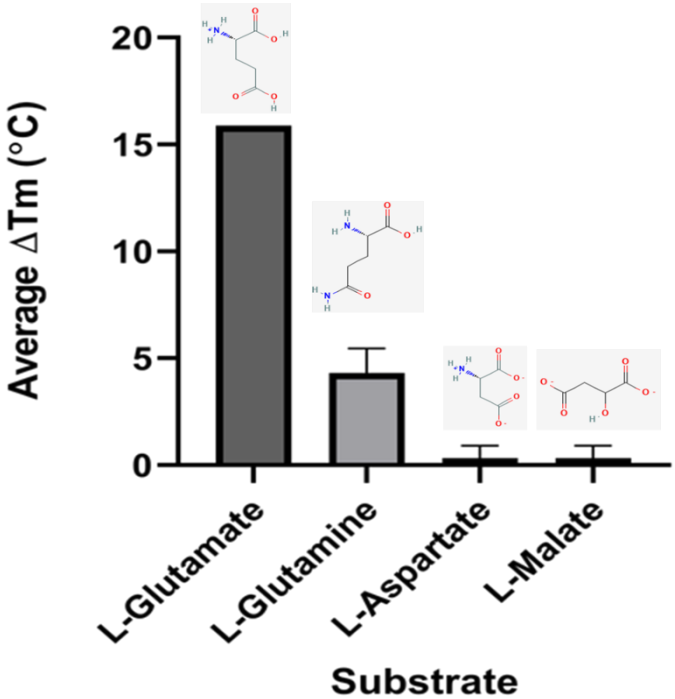

Figure 12 ***ΔTm of different C4 Carboxylates.*** *A bar chart plotting the average ΔTm and standard deviation for different substrates (above each bar) with no clear increase seen with L-aspartate or L-malate which indicates no binding activity. Standard deviation was too small to be visible for L-glutamate. Each substrate was tested in triplicate.*

3.2.3 Assessing the stereoselectivity of VC0430 binding

Although we have strong evidence that VC0430 binds L-glutamate and L-glutamine, the high ΔTm seen in the presence of L-glutamate or L-glutamine in comparison to the almost 0 °C ΔTm seen with the structurally similar C4 Dicarboxylates tested, suggesting that they do not bind (Figure 13) and that VC0430 is also highly specific for L-glutamate and L-glutamine. As such we tried to determine if VC0430 would bind the rarer D enantiomers of glutamate and glutamine that are not typically found in nature. DSF was repeated with the D enantiomers of glutamate and glutamine, resulting in a substantial ΔTm seen in the presence of 1 mM D-glutamate, although much lower than that seen in the presence of 1 mM L-glutamate, suggesting that VC0430 can still bind D-glutamate (Figure 15A). Based on our previous observation that higher concentrations of glutamine were required to observe a significant ΔTm, higher concentrations of D-glutamine were used (1 mM, 5 mM and 15 mM). Only a very small ΔTm of -7.63E-06 ± 0.468 °C was seen in the presence of 1 mM and 5 mM but a more significant ΔTm of 2.318 ± 2.55E-04 °C was seen in the presence of 15 mM D-glutamine despite being much lower than what was seen with L-glutamine (Figure 15B). These data indicate that VC0430 can bind D-glutamine and D-glutamate but only when the ligands are present at a high concentration suggesting that VC0430 has a considerably lower affinity for the D enantiomers of glutamate and glutamine compared to the L enantiomers.

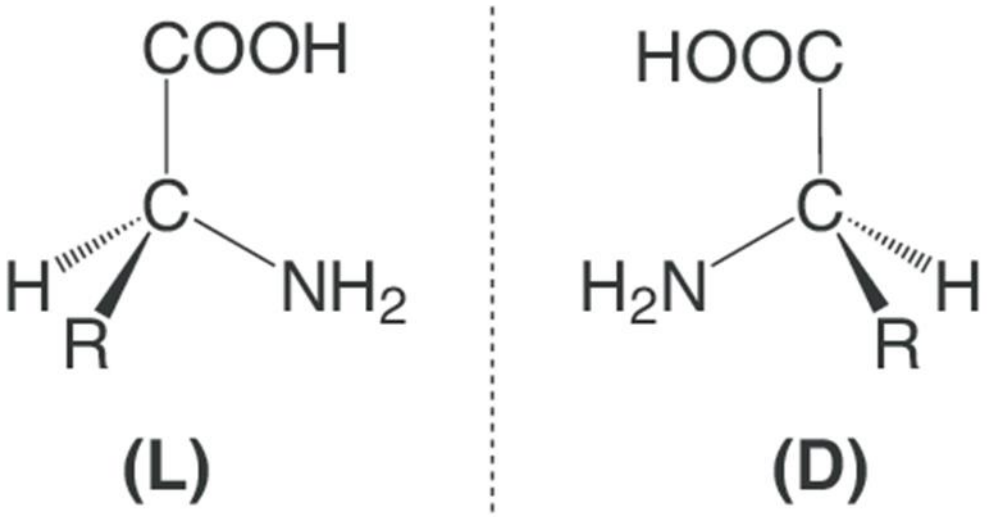

Figure 14 ***D and L amino acids****. A schematic showing the D and L enantiomers of amino acids. They are mirror images of each other and therefore have a different arrangement of atoms in 3D space.*

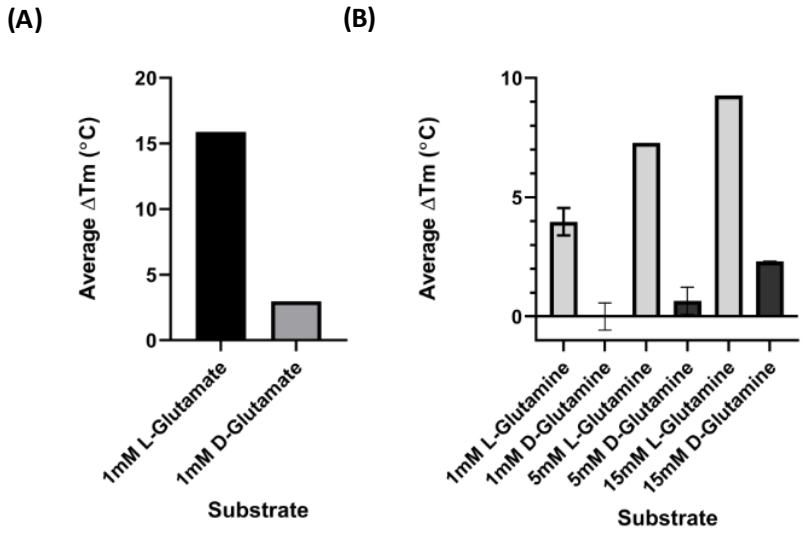

Figure 15 ***Binding of the D and L enantiomers of glutamate and glutamine****. Bar chart of average ΔTm for 1 mM D and L glutamate (A) Bar chart of average ΔTm for a variety of concentrations of D and L glutamine (B). Due to the much lower affinity of VC0430 for L-glutamine much higher concentrations of D-glutamine were required to see any significant change of ΔTm. Standard deviation displayed by error bars except when the error was too small to be visible. Each substrate was tested in triplicate.*

3.3 Intrinsic Tryptophan Fluorescence

While DSF can provide an indication of which substrates a protein can bind it is not possible to obtain a specific affinity without considerable modification, so a different assay was sought. Tryptophan fluorescence has been used extensively for SBP characterisation(5,16,35). The fluorescence of tryptophan changes based on the environment that it is in(36). Therefore, a conformational change in response to ligand binding would result in either an increase in (enhancement) or decrease in fluorescence (quenching), due to the environment of the tryptophan being altered. As such ligand binding can be measured by a change in the fluorescence of tryptophan.

3.3.1 3D Model of VC0430 Shows Location of Two Tryptophan Residues

In order to locate the tryptophans in the Vc0430, we needed the 3D structure of the protein. In the absence of a crystal structure for VC0430, we generated a model using Phyre2 revealing a template of an immunogenic protein from *Ehrlichia chaffeensis* (PDBe: 4ddd), giving 100 % confidence but with only 31 % sequence id. Another structure of a TAXI-TRAP Transporter that has been solved is a glutamate bound periplasmic glutamate/glutamine binding protein (TtGluBp) in *Thermos thermophilus* (PDBe: 1us5). Overlaying the two structures reveals the potential ligand binding site for VC0430 as well as the position of two tryptophan's in relation to this potential binding site: tryptophan 96 and tryptophan 170 (Figure 16). However, tryptophan 96 is likely to contribute more to a fluorescence reading as it is much closer to the potential binding site than tryptophan 170.

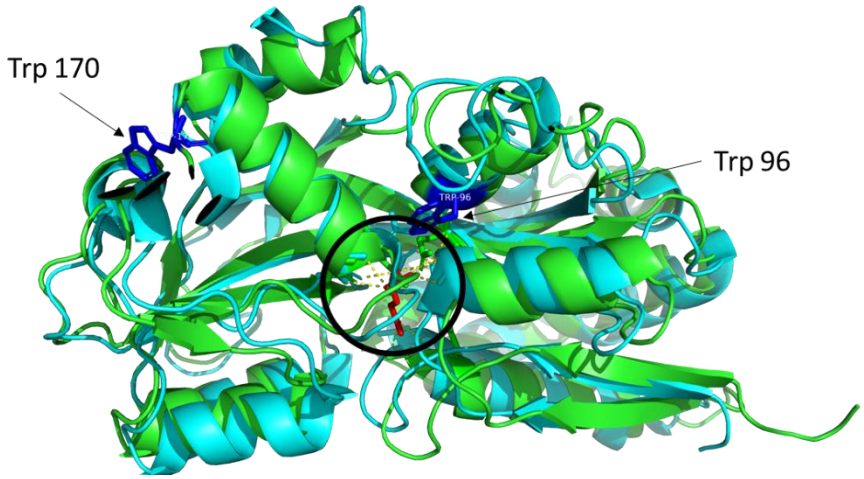

Figure 16 ***Locations of tryptophans in VC0430****. Overlayed 3D model of VC0430 (green) and the solved structure of the glutamate/glutamine SBP from Thermos thermophilus 1us4 (cyan). Tryptophan residues of VC0430 shown in blue. Bound glutamate shown in red and potential binding site circled.*

3.3.2 Initial VC0430

Emission Scans

There is a good chance that these tryptophans can be used to report on ligand binding. To test this, we performed and emission scan between 300nm and 400nm with an excitation wavelength of 295 nm, which will specifically excite tryptophan residues(37). However, initial emission scans we performed of VC0430 with DL-glutamate proved only partially successful. In the presence of no substrate a clear curve could be seen between an emission wavelength of 300nm and 400nm which is typical of tryptophan emission(37) with a peak at 330nm, but upon addition of substrate, no change in fluorescence was observed (Figure 17) despite clear binding seen in the DSF. Based on this unexpected result we reasoned that the large 6.5 kDa 10x His-FLAG-TEV tag could be interfering with the binding site in the tryptophan fluorescence as an enhancement of fluorescence has been observed with a variant of this protein with a shorter His-tag at the C-terminus end (C. Mulligan, personal communication). In DSF the protein reaches high temperatures of close to 100°C. At these high temperatures it is possible that the tag has enough kinetic energy to be displaced from the binding site and allow the correct substrate to bind. For the tryptophan fluorescence we kept at a temperature of approximately 20°C which would mean the tag would have significantly less kinetic energy and as such would possibly be unable to dislodge from the binding site and allow the correct substrate to bind. To test this theory, we removed the FLAG and His tag with TEV protease, leaving just VC0430 (See Figure 9 for a schematic of VC0430).

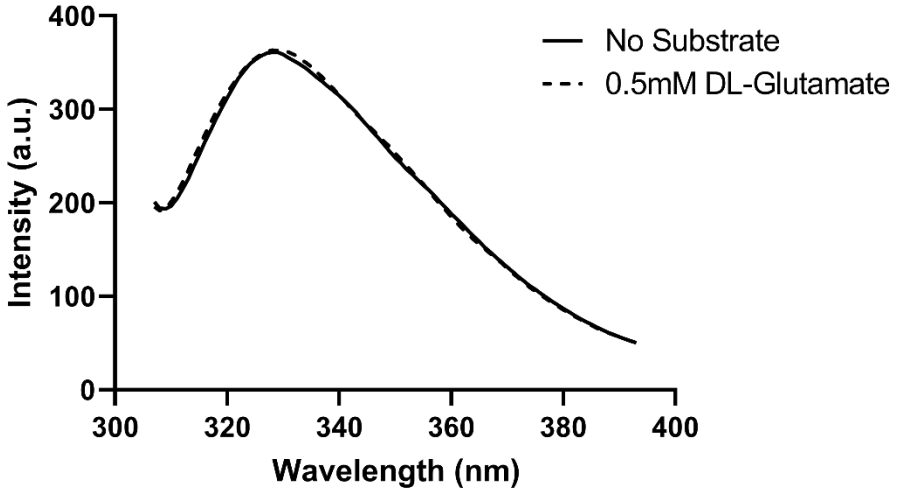

Figure 17 ***Tagged VC0430 Emission Scan Spectra****. Intrinsic Tryptophan Flourescence Emission Scan Spectra for VC0430 with (dashed line) and without (solid line) the presence of 0.5 mM DL-glutamate. Despite binding data from DSF only an enhancement of 0.664 % was seen. Repeated on 3 separate occasions.*

3.3.3 Removal of the FLAG and His Tag with TEV Protease.

For us to remove the tag on VC0430 we determined that TEV protease was the best option to cleave the tag off due to the built-in TEV Cleavage site. The TEV Protease was part of a plasmid also containing a Maltose Binding Protein (MBP) (Plasmid prk793, see methods). This MBP is fused to TEV (Figure 18) in an effort to help solubilize and fold the TEV when it is produced in *E.coli* in order to increase protein yield(38). After this fusion protein is produced the MBP is cleaved off at a built in TEV site, leaving pure TEV (39).

3.3.3.1. Production and Purification of TEV Protease

We purified TEV following a 2-step purification process with Nickle affinity chromatography (see methods for details). The flowthrough (FT) and wash (W) stages of the first step along with the FT and final protein elution stages of step 2 were all ran on an SDS gel together and stained with Coomassie Blue. We observed how a lot of the MBP was present on the first flowthrough, but much of it was still present in the wash and second flowthrough (Figure 19). However, in the final elution the majority of the MBP was removed, leaving pure TEV (Figure 19). Despite lots of TEV seeming to be present in the flowthrough and wash, indicating that not all the TEV bound to the resin, enough was able to

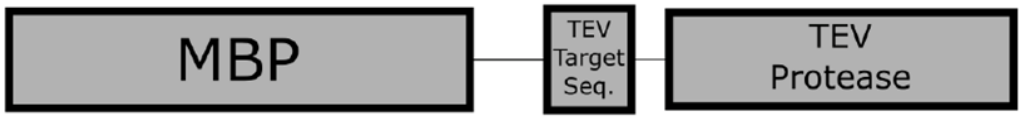

Figure 18 ***Schematic of the TEV-MBP construct.*** *The TEV-MPB construct with the position of the TEV target sequence. After production of the construct the TEV cleaves of the MBP at the target sequence, leaving pure TEV protease remaining.*

be purified to attempt cleavage of the VC0430 tag.

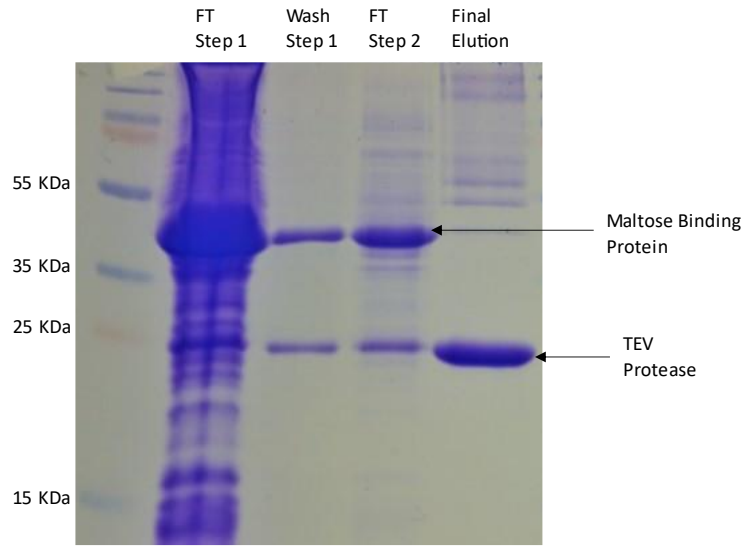

Figure 19 ***Production of TEV protease****. SDS PAGE stained with Coomassie Blue of TEV protease purification. The purification process requires two steps of purification on the IMAC column. The plasmid produces TEV with a Maltose Binding Protein that helps fold the TEV which is removed in the second step of purification.*

3.3.4. TEV Protease Cleavage Optimisation

Once TEV Protease had been produced and purified, we observed that the protocol produces much less protein than VC0430 and as such a trial of different molar ratios of TEV with 0.5nmol of VC0430 was tested to optimise the cleavage reaction to use the least amount of TEV while still obtaining full cleavage. We tested a range of ratios from 2120:1 to 265:1 of TEV:VC0430 (Figure 20). Each sample of VC0430 was incubated with the appropriate amount of TEV and left overnight mixing at 4°C before using SDS-PAGE to analyse the samples the next day. The SDS gel revealed that across all the ratios tested, TEV is effective at completely removing the tag from VC0430. Further experiments could be done to assess the effectiveness of TEV at molar ratios of less than 265:1 but for our purposes we observed that adding TEV in at least a 265:1 ratio was enough for full cleavage of VC0430 while saving on TEV. However, to speed up the whole purification and tag removal process we decided to incubate the VC0430 with TEV for three hours at room temperature instead of overnight at 4°C which proved effective in completely removing the tag on VC0430. However, because of another protein (TEV) being added to VC0430, an extra step of purification by

Size Exclusion Chromatography (SEC) was performed to assess the quality of the VC0430 after these manipulations. A defined peak was seen (Figure 21A) encompassing the elution fractions C6, C7, C8, D1 and D2 from a 48-Tube sample collector (Figure 21B). SDS-PAGE was then used to assess the protein contents of each SEC elution where we observed how only VC0430 was present, confirming that we had removed the tag and separated the TEV and VC0430 (Figure 21B,22).

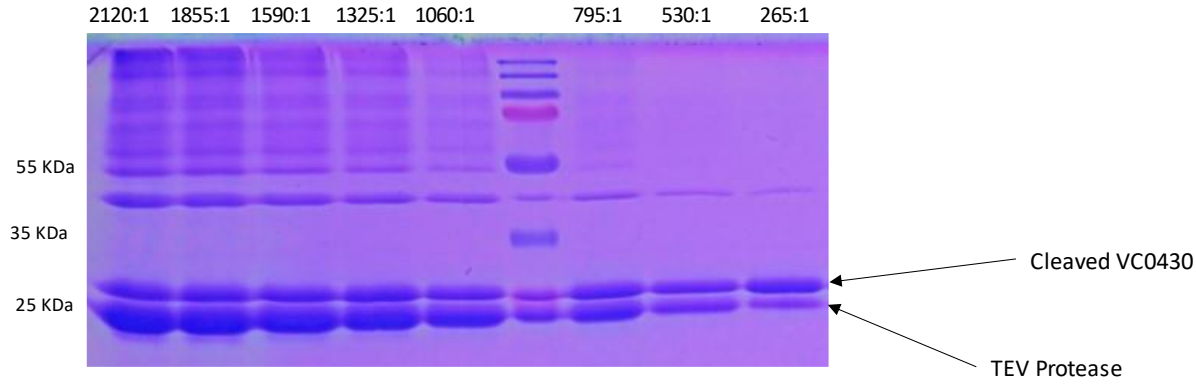

Figure 20 ***TEV Protease Optimization****. SDS PAGE of VC0430 with decreasing molar ratios of TEV Protease to VC0430 (Wells 1-5, 7-9) with tag-free VC0430 and TEV protease labelled. Note: some spillage occurred from well 5 resulting in the presence of TEV and VC0430 in the lane containing ladder.*

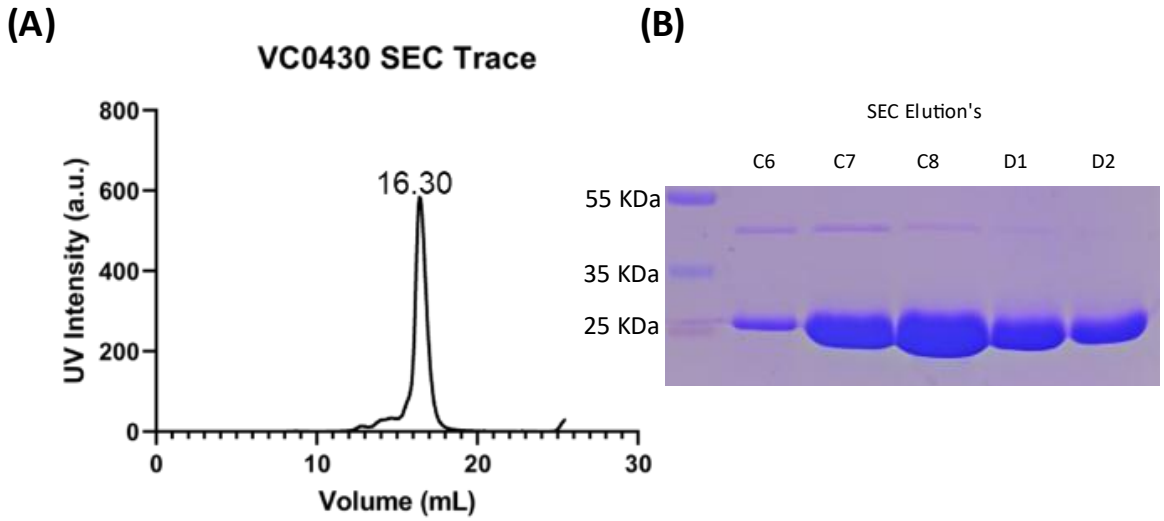

Figure 21 ***SEC Purification of VC0430. (A)*** *SEC Trace of VC0430 after refolding and incubation with TEV. A clear peak with no other peaks indicates that the protein is folded and stable. (B) SDS PAGE showing purified SEC Elutions, giving pure, tag-free VC0430 without the presence TEV.*

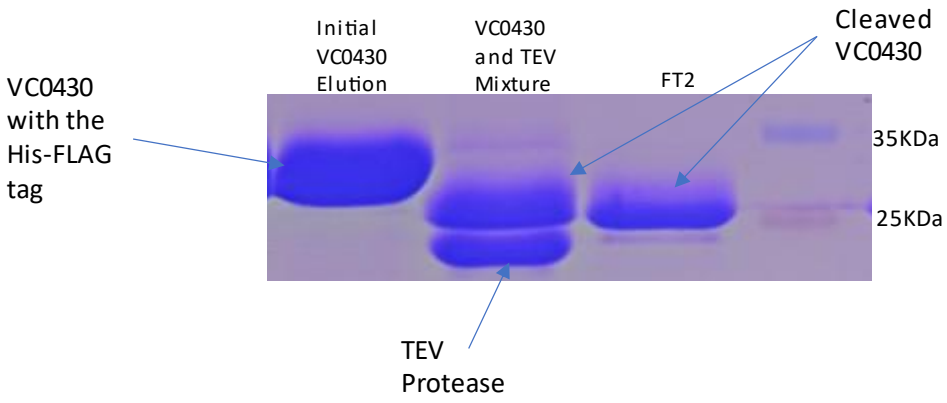

Figure 22 ***Purification of tag-free VC0430****. SDS PAGE showing the initial purification of tagged VC0430, the addition of TEV protease and the second stage purification Flowthrough (FT2) where the tag-free VC0430 was separated from TEV and collected.*

3.3.5. VC0430 Emission Scans with Tag Free Protein

We then repeated the fluorescence emission scans but this time with tag free VC0430 as described previously. In the absence of the tag, we observed a well-defined curve from emission wavelengths of 300nm and 400nm that we had seen before with tagged protein, confirming that removing the tag had not drastically affected the initial emission spectra of VC0430. We then repeated the emission scans in the presence of 50 µM DL-glutamate or 100 µM L-glutamine and an enhancement of approximately 9.14 % or 4.94 % respectively at an emission wavelength of 330nm (Figure 23). Typically, an enhancement of intrinsic tryptophan fluorescence is seen when the tryptophan residues polar environment changes drastically(36), the enhancement seen here for DL-glutamate and L-glutamine suggests that they bind VC0430 and is likely a result of a conformational change of the residues around the binding site closing around the substrate that typically takes place in other SBPs(40). As such, it is likely that Trp-96 is mostly responsible for the enhancement seen as it is near the binding site so a conformational change of the protein that then changes the environment of the residues around the binding site would be more likely to drastically alter the environment of Trp-96, resulting in an enhancement of the fluorescence signal which suggests that the tag was inhibiting substrate binding.

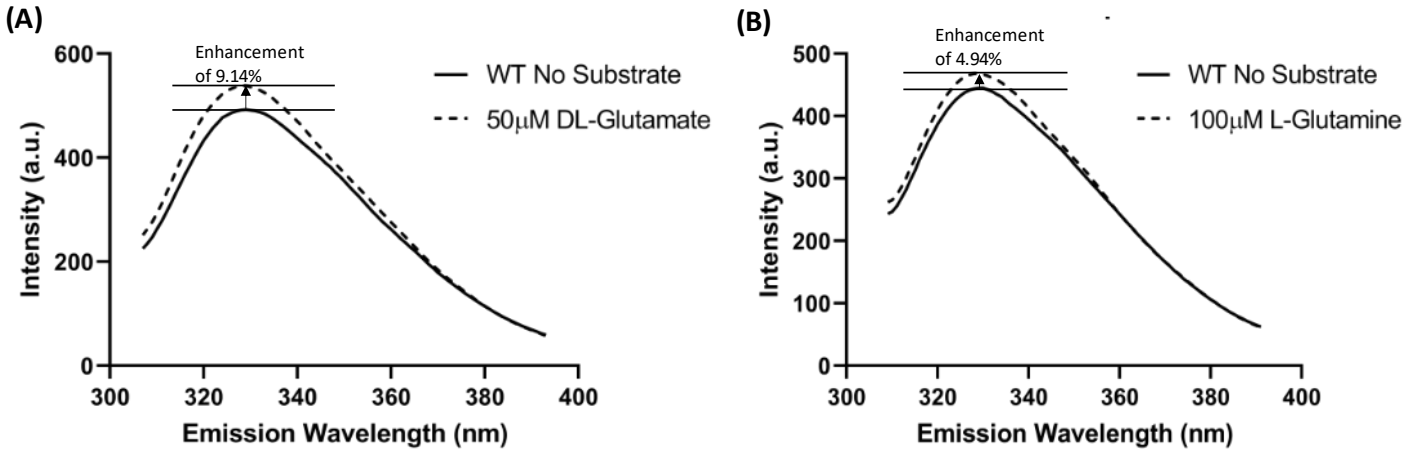

Figure 23 ***Tag free VC0430 emission spectra****. Intrinisc Tryptophan Fluorescence Emission Scan Spectra of VC0430 with (dashed line) and without (solid line) 50 μM DL-glutamate (A) or 100 μM L-glutamine (B). With DL-glutamate it appears as a bigger enhancement of 9.14 % was seen compared to the enhancement of 4.94 % seen in the presence of L-glutamine. Each experiment was repeated twice.*

3.3.6. VC0430 L-Glutamate and L-Glutamine Titrations

Based on the enhancement seen in the emission scans we decided to use this change in fluorescence intensity to estimate the Kd of VC0430 for L-glutamate and L-glutamine. We added consecutive different concentrations of either substrate to saturate binding which was determined when no additional enhancement was observed. The difference in fluorescence (Δfluorescence) was then calculated based on the initial fluorescence signal with no substrate for each addition of substrate to construct a binding curve (see methods Figure 7). We then used non-linear regression with the One Site Total Binding model (Y = Bmax*X/(Kd + X)) in GraphPad Prism to get an estimate of the Kd. For L-glutamate we determined Kd of 0.10 ± 0.051 μM from a total of 11 titrations and for L-glutamine we determined a Kd of 18.53 ± 6.78 μM from a total of 6 titrations. Based on these estimates it appears that glutamine has a Kd of approximately 180 times that for L-glutamate. This strongly suggests that glutamate is the primary substrate, and that L-glutamine is a possible unintended secondary substrate as a consequence of its similarity to L-glutamate.

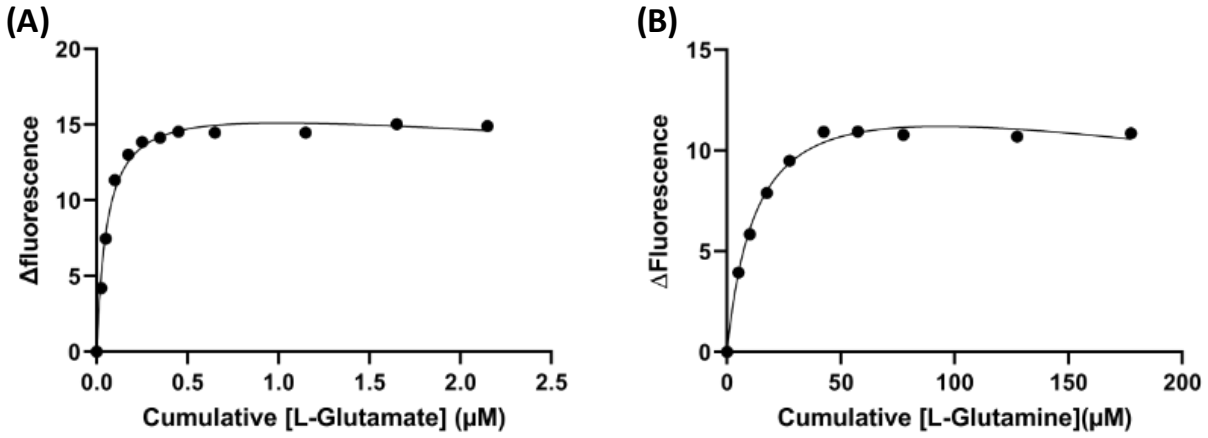

Figure 24 ***L-glutamate and L-glutamine WT titrations****. Representative Binding curves for L-glutamate (A) or for L-glutamine (B) fitted to the "One Site Total Binding" model. The L-glutamate binding curves gave and estimated Kd of 0.10 μM with a Standard Deviation of 0.051 and a Standard Error of the Mean of 0.0155 from 12 separate titrations. The L-glutamine binding curves gave an estimated Kd of 18.53 μM with a Standard Deviation of 6.78 and a Standard Error of the Mean of 2.77 from 6 separate titrations. A slight decrease can sometimes be observed due to VC0430 being completely saturated at higher concentrations resulting in incredibly minor changes in fluorescence that can appear to be higher or lower than the saturation point. Additionally, at higher concentrations the assay has been running for a much longer time so some photobleaching may occur, resulting in a decreased signal.*

3.3.7 VC0430 D-Glutamate and D-Glutamine Titrations

As seen in the previous DFS data, it appears that VC0430 likely binds both the D and L form of both glutamate and glutamine. However, it was unclear if VC0430 binds the D enantiomers with a different affinity. To confirm this, we performed the same titrations but with the D enantiomers of glutamate and glutamine instead. For D-glutamate we determined a Kd of approximately 24.51 ± 10.15 μM from 9 titrations which was even higher than the estimated Kd for L-glutamine. However, we could not determine a Kd for D-glutamine as no significant enhancement signal could be seen. Therefore, it is possible that VC0430 has some flexibility in substrate specificity but within a narrow range.

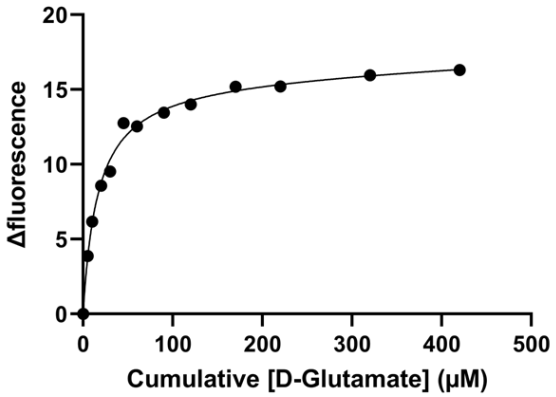

Figure 25 ***D-glutamate WT titration****. Representitive Binding curve for D-glutamate fitted to the "One Site Total Binding" model. The Kd was estimated as 24.514 μM with a Standard Deviation of 10.150 μM and a Standard Error of the Mean of 3.383 μM from 9 separate titrations.*

3.4. Site Directed Mutagenesis

3.4.1. Selecting Residues to Mutate

Having established the fluorescent properties of VC0430 wild type and an estimation of the Kd the next step was to select residues in the predicted binding site of the VC0430 model to mutate to alanine to determine which residues are essential for binding L-glutamate and L-glutamine.

To find key binding residues the generated model of VC0430 was overlayed on to the solved structure of another TAXI-TRAP SBP bound to glutamate glutamine and overlapping residues were selected (Figure 26). Six clusters (1-6) of residues from left to right around the bound L-glutamate in TtGluBp were identified (Figure 26, Table 12). The backbone of cluster 1 involving residues interacts with the top oxygen on the delta carbon and the hydroxyl group from the side chain of Y32 interacts with the amine group of glutamate (Figure 26A). In cluster 2, the delta carbon hydroxyl group of E111 interacts with the amine group of glutamate (Figure 26B). In cluster 3, the carbonyl group of the sidechain of Q78 interacts with the amine group of glutamate (Figure 26C). In cluster 4, the amine group of T187 interacts with the amine group of glutamate (Figure 26D). In cluster 5, the hydroxyl group of T143 and the backbone interact with the bottom oxygen of glutamate (Figure 26E). In cluster 6 the hydroxyl group in the side chain of S60 as well as the backbone interact with the top oxygen of the carboxylate group of glutamate (Figure 26F). Based on these clusters, 5 specific residues protrude into the binding cavity and have side chain elements directly interacting with glutamate: Y45, Q93, E125, Y200 and M201.

Table 12 ***VC0430 substrate binding clusters****. A table showing the key residues that make up the binding clusters in TtGluBp and corresponding residues in VC0430.*

Cluster	Residues in TtGluBp	Corresponding residues in VC0430	Section of Figure 26
1	Glycine 30 Valine 31 Tyrosine 32	Glycine 43 Valine 44 Tyrosine 45	A
2	Glutamic acid 111	Glutamic acid 125	B
3	Alanine 77 Glutamine 78	Valine 92 Glutamine 93	C
4	Tyrosine 186 Threonine 187	Tyrosine 200 Methionine 201	D
5	Glycine 142 Threonine 143	Glycine 156 Aspartic acid 157	E
6	Glycine 59 Serine 60	Glycine 74 Serine 75	F

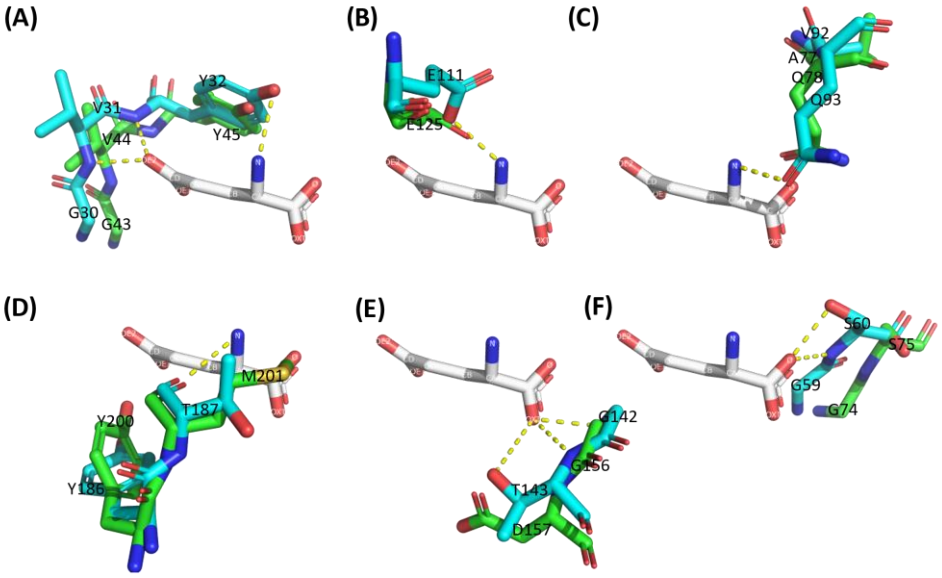

Figure 26 ***Position of VC0430 binding clusters around substrate****. Overlapping residues of VC0430 in the binding site of TtGluBp with bound glutamate (grey). TtGluBp in cyan and VC0430 in green. The yellow dashed lines show polar contacts determined by PyMol. Binding cluster 1(A). Binding cluster 2 (B). Binding cluster 3 (C). Binding cluster 4 (D). Binding cluster 5 (E). Binding cluster 6 (F).*

3.4.2 Production and Purification the VC0430 Mutants

We then mutated each selected residue to alanine by site directed mutagenesis and the gene was then expressed following the same protocol as wild type VC0430. However, although we denatured VC0430 WT to remove any pre-bound ligand, there was no significant evidence that large amounts of ligand were prebound we decided to skip this step for the mutants, especially as an initial experiment we performed with refolded mutants had resulted in extremely poor protein yield. All mutants, except the tyrosine mutant Y200A, produced a similar yield of protein to WT based on the SDS-PAGE analysis (Figure 27). The lower yield of Y200A indicated that the mutation had a greater impact on the overall fold of VC0430, possibly causing aggregation so the protein could not be harvested. Furthermore, DSF of all the mutants revealed a Tm that was less than WT, suggesting that all the mutations had an impact on the stability of the protein (Figure 28).

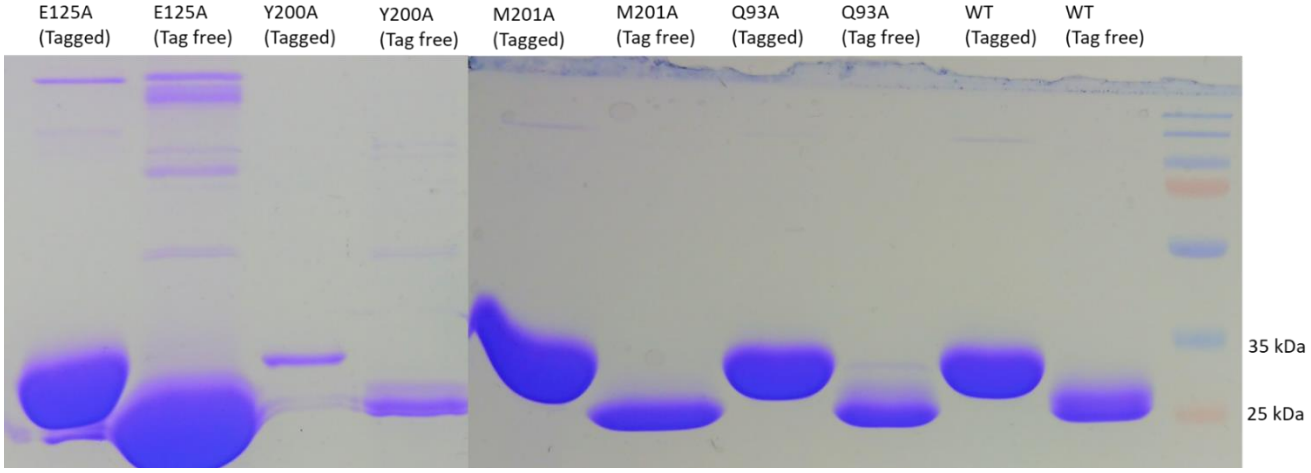

Figure 28 ***Purification of VC0430 Mutants****. SDS-PAGE of four of the mutants from left to right: E125A, Y200A, M201A and Q93A with VC0430 WT as a control. Mutant Y45A not shown. For each mutant, one lane was loaded with tagged protein before TEV cleavage and the next lane was tag free protein after TEV cleavage.*

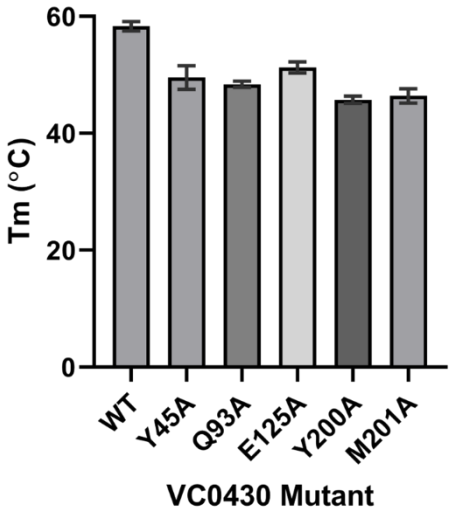

Figure 27 ***Tm's of all Mutants****. A bar chart showing the average melting temperature (Tm) of each mutant in the absence of ligand with the standard deviation displayed as error bars. The average Tm for all samples was calculated from two triplicates (6 individual Tm's).*

3.4.3. DSF Screen for Binding Activity of the Mutants

To initially screen the mutants to see if they still showed binding activity, we used DSF in the presence of 1 mM DL-glutamate or L-glutamine. We observed how an addition of 1 mM DL-glutamate resulted in a significant ΔTm for all mutants except for Y200A (Figure 29A) and an addition of 1 mM L-glutamine resulted in a significant ΔTm for all mutants except for Y200A and Q93A (Figure 29B). We concluded that Y200A had completely knocked out all substrate binding of glutamate and glutamine and that Q93A had only inhibited glutamine binding. To confirm if this was the case with Q93A, we repeated the DSF but with a higher concentration (10 mM) of L-glutamine for all mutants which resulted in a higher ΔTm by approximately 2 °C for all mutants except Y200A (Figure 30), indicating that perhaps Q93A could still bind L-glutamine but at a higher concentration. These initial experiments therefore show how Q93 and Y200 in VC0430 are likely key residues for substrate binding and specificity.

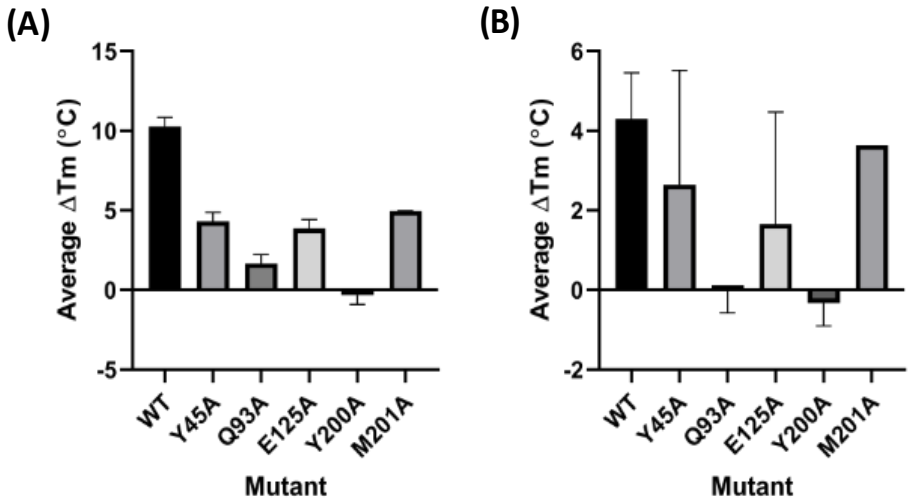

Figure 30 ***Average ΔTm of VC0430 mutants for L-glutamate and L-glutamine****. Bar Charts of average ΔTm with 1 mM DL-glutamate (A) or 1 mM L-glutamine (B). All mutants show binding activity at 1 mM of substrate except mutants Y200A and Q93A with L-glutamine. Standard deviation shown as error bars unless the error was too small to be seen. Each experiment was repeated 3 times*

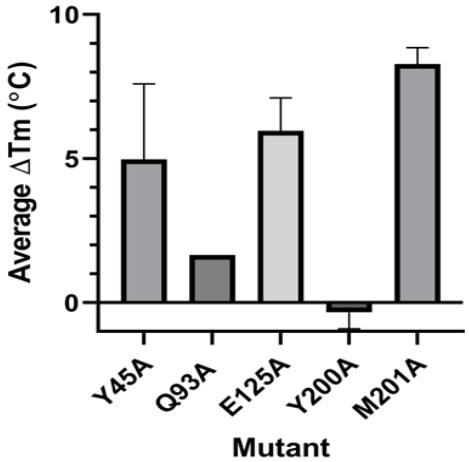

Figure 29 ***Average ΔTm of VC0430 mutants with 10 mM L-glutamine****. Bar Chart of average Tm for all mutants with 10 mM L-glutamine. At this higher concentration potential binding activity can be seen for mutant Q93A. Standard deviation shown as error bars unless the error was too small to be seen. Repeated 3 times.*

3.4.4 Intrinsic Tryptophan Fluorescence

After confirming which mutants exhibit binding activity in the DSF screen (Y45A, Q93A, E125A and M201A) they were then confirmed with fluorescence emission scans. We repeated fluorescence emission scans following the same protocol as with the wild type VC0430 for L-glutamate and L-glutamine, and gave similar emission spectra to wild type, with the peak of fluorescence intensity being around 330nm, but surprisingly, a larger enhancement was observed for all mutants except Y200A (Figure 31). A small enhancement was seen with Y200A, but it was too small to gain any meaningful information from it. This is further evidence that the Y200A mutation has completely wiped out any binding activity.

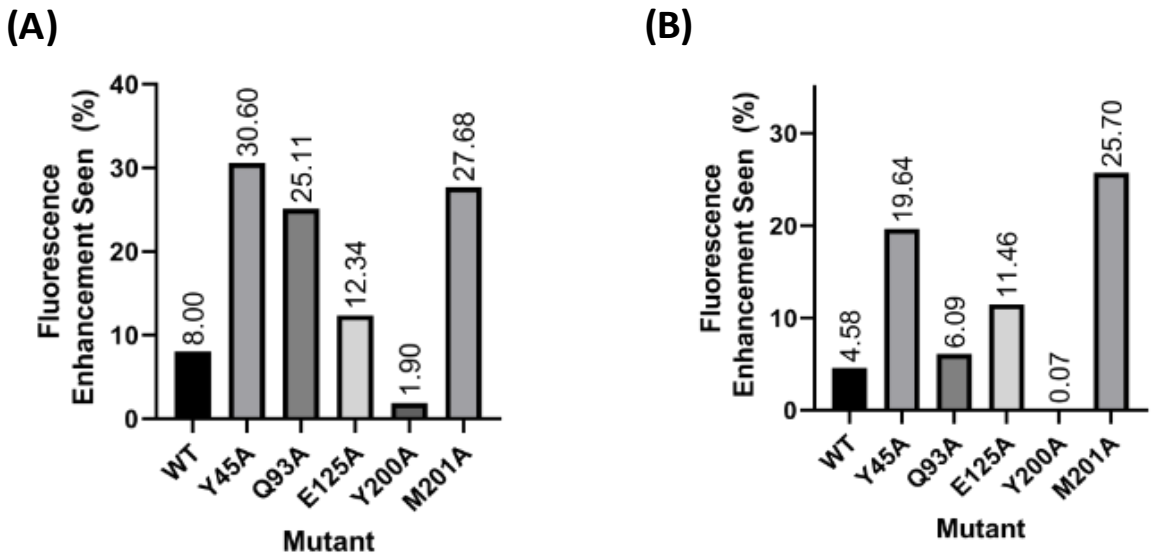

Figure 31 ***Maximum enhancement of VC0430 mutants****. Bar Charts showing the maximum percentage enhancement seen (number above each bar) with DL-glutamate (A) or L-glutamine (B) for all mutants. All mutants except Y200A show some considerable enhancement compared to wild type except mutant Y200A. Value displayed was the greatest enhancement seen from at least 3 repeats.*

3.4.5. Intrinsic Tryptophan Fluorescence Titrations With L-Glutamate

After establishing which mutants bind DL-glutamate and L-glutamine and still display detectable fluorescent properties, we performed titrations to estimate the Kd of each mutant. However, as DL-glutamate was used in the DSF and initial emission scans as they were both qualitative experiments, for estimating the Kd of all the mutants we only used the L enantiomers of each substrate. For binding L-glutamate, it appears that all mutations except Y200A still exhibited L-glutamate binding activity but with reduced affinity (Table 13). We observed how the mutants E125A and M201A still bound L-glutamate with a high affinity but 2-3 times less than wild type, suggesting that M201 and E125 are not vital residues for substrate binding. On the other hand, mutants Y45A and Q93A were observed to have

a significantly lower affinity for L-glutamate than wild type, with a Kd approximately 150 times and 700 times less respectively than wild type, suggesting that they are much more important for substrate binding.

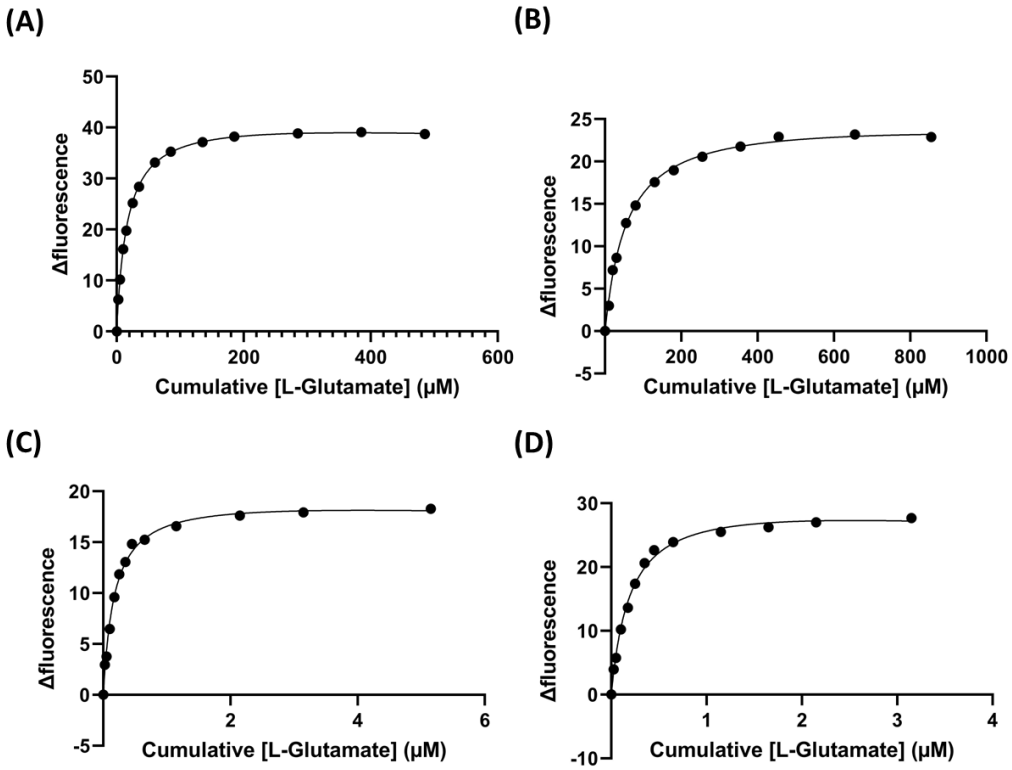

Figure 32 ***Representitive titrations of L-glutamate for VC0430 mutants.*** *Representative binding curves for each mutant fitted to the One Site Total Binding model: (A) Y45A (B) Q93A (C) E125A (D) M201A.*

Table 13 ***L-glutamate average Kd's for VC0430 mutants.*** *A table showing Average Kd with Standard Deviation, Standard Error of the Mean and Number of Titrations performed of each mutant for L-glutamate.*

Mutation	**Average KD (μM)**	Standard Deviation	SEM	Number Of Titrations
WT	**0.103**	0.051	0.016	11
Y45A	**15.820**	1.579	0.706	5
Q93A	**74.925**	17.782	5.623	10
E125A	**0.272**	0.110	0.045	6
Y200A	**N/A**	N/A	N/A	N/A
M201A	**0.328**	0.099	0.044	5

3.4.6. Intrinsic Tryptophan Fluorescence Titrations With L-Glutamine

We then performed L-glutamine titrations of the mutants to see how the mutations had specifically impacted L-glutamine binding. In the presence of L-glutamine we observed how most of the mutants showed similar binding capacities to what we saw with L-glutamate binding (Table 14). We determined that E125A and M201A both have a Kd approximately 2-3 times that of wild type similar to what we observed with L-glutamate binding. Mutant Y45A

also shows a considerably higher Kd as seen with L-glutamate, but with a relatively lower Kd, approximately 450 times the Kd of WT as opposed to 700 times that was seen with L-glutamate. However, it was surprising to see that with mutant Q93A, despite displaying some potential binding activity in DSF and some enhancement in the emission scans, a titration with L-glutamine could not be performed for Q93A.

We noted how highly concentrated additions of L-glutamine would result in a minor enhancement before continuously quenching to below the no substrate baseline (Figure 33). When we repeated the same experiment with the same concentrations of L-glutamine for WT where we saw the same trend but with a greater enhancement initially. As such it was deemed not possible to perform a titration with Q93A as the initial enhancement was far too small. Thus, it highlights the crucial role of Q93 in VC0430 for potentially binding L-glutamine.

Table 14 ***L-glutamine average Kd's for VC0430 mutants.*** *A table showing average Kd with Standard Deviation, Standard Error of the Mean (SEM) and Number of Titrations for each mutant for L-glutamine.*

Mutation	**Average KD (µM)**	Standard Deviation	SEM	Number Of Titrations
WT	**18.525**	6.782	2.769	6
Y45A	**8665.333**	2603.739	1164.428	6
Q93A	**N/A**	N/A	N/A	N/A
E125A	**36.754**	13.912	6.222	5
Y200A	**N/A**	N/A	N/A	N/A
M201A	**48.638**	15.694	5.231	9

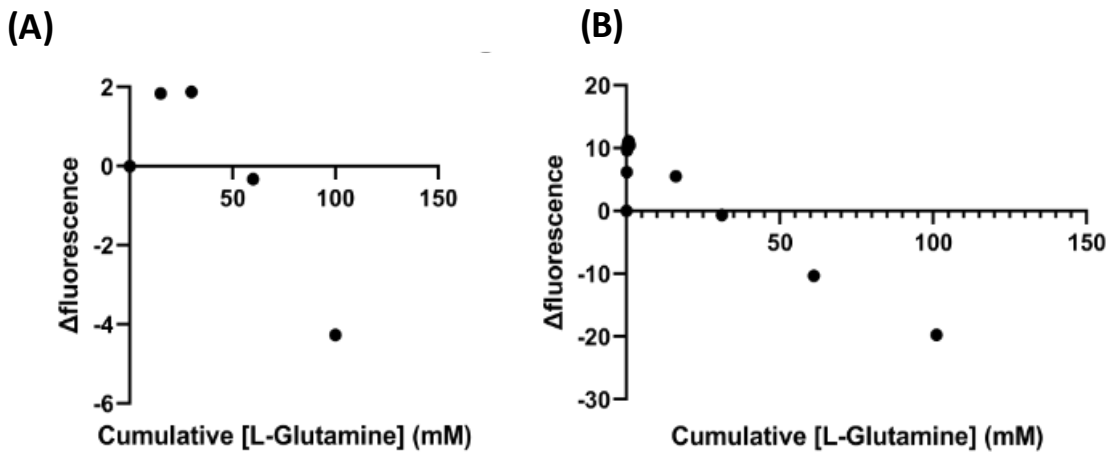

Figure 33 ***L-glutamine fluorescence quenching****. Graphs of Δfluorescence against Cumulative [L-glutamine] (mM) for VC0430 mutant Q93A (A) or Wild Type (B). For both Q93A and WT a cumulative [L-glutamine] of >=50 mM resulted in large relative quenching. However (B) has an initial Δfluorescence of close to 10 as compared to 2 seen in (A) so a titration was able to be performed within this range but not for Q93A*

3.5. Protein Crystallography

As mentioned previously, currently the only known structure of TAXI-TRAP transporter SBP is the protein TTGluBp in Thermus thermophilus in a study by H. Takahashi et al.(27). As such, it makes it difficult when trying to biochemically characterise other TAXI-TRAP SBPs, often having to resort to generated models which prevents a completely thorough understanding of substrate binding in these proteins. We decided to crystallize VC0430 in different defined conditions: without substrate (*apo*), with L-glutamate and with L-glutamine to solve the structure and get a more thorough understanding of specific substrate interactions in the binding site.

3.5.1. Initial 96-Well Plate Screens

To try and find the best conditions for crystallization of VC0430 at a concentration 15 mg/mL we first set up two 96 well plates with different conditions in each well from the screening kits: JSCG+ and Wizard Classic from Molecular Dimensions. Most wells were unsuccessful, but we were able to observe a single large crystal that had been formed in one well which contained 2.4 M Sodium Malonate Dibasic Monohydrate (SMDM, Condition 2-21 of JCSG+) (Figure 34A). After, leaving the well for an even longer time, more large crystals had formed (Figure 34B) highlighting 2.4 M SMDM as key crystallization condition that we should screen around.

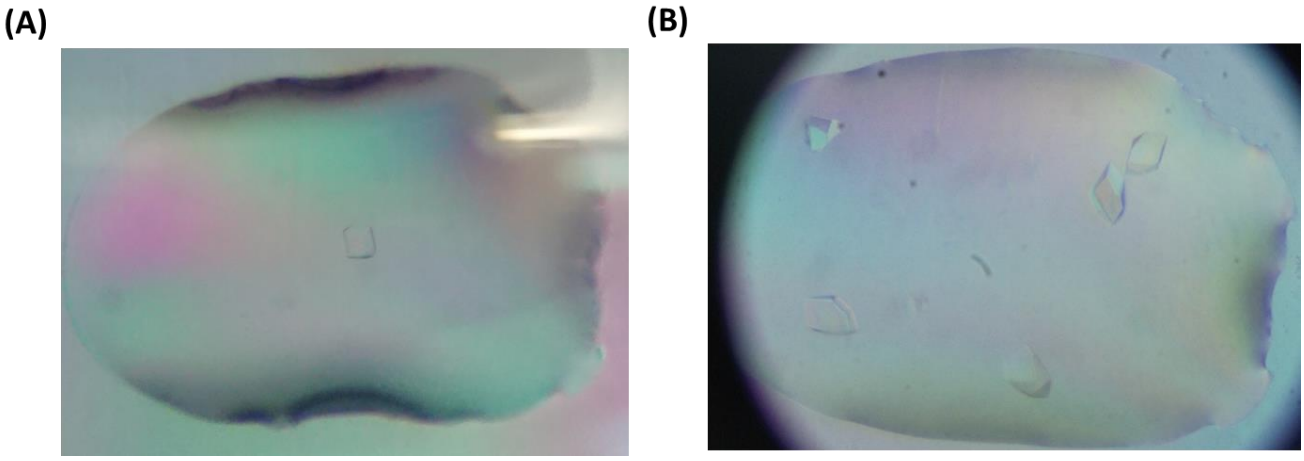

Figure 34 ***VC0430 initial crystal screen.*** *Initial crystal seen in 96-Well Plate screen in condition 2-21 of JCSG+ (A) and same well 2 weeks later (B). Initially only one crystal could be seen but leaving the well for an additional 2 weeks resulted in the formation of even more crystals, highlighting this condition as a strong option of crystallising VC0430. Photos taken at 96x magnification.*

3.5.2. 24-Well Plate Protein Crystallization Condition Optimisation

Next, we set up 24-Well plate with 2.4M SMDM to see if protein crystals would still form in a bigger droplet size with a 1:1 ratio of protein and 2.4M SMDM in the hanging drop. The plate was then checked after 2 days revealing many, large cube-like crystals (Figure 35). We then preceded to try and co-crystallize VC0430 with L-glutamate and L-glutamine bound by incubating VC0430 with different concentrations of the corresponding substrate. At a ratio of 1:1 of VC0430 to SMDM with either 1 mM of L-glutamine or 0.5 mM L-glutamate we noted the formation of many large crystals (Figure 36). Interestingly, although we observed large crystals for each substrate, considerably more were seen in the presence of L-glutamate instead of L-glutamine which is likely indicative of VC0430's higher affinity for L-glutamate and how substrate binding has potentially increased the stability of VC0430 allowing the formation of more crystals.

Based on these observations we concluded that the best conditions for the crystallization of VC0430 is 2.4M SMDM at a 1:1 ratio with VC0430 at a concentration of 15 mg/mL. We have been very successful with these crystals and currently have large amount to be diffracted. However, we have not yet determined how well these crystals will diffract which remains as the next major step in this project.

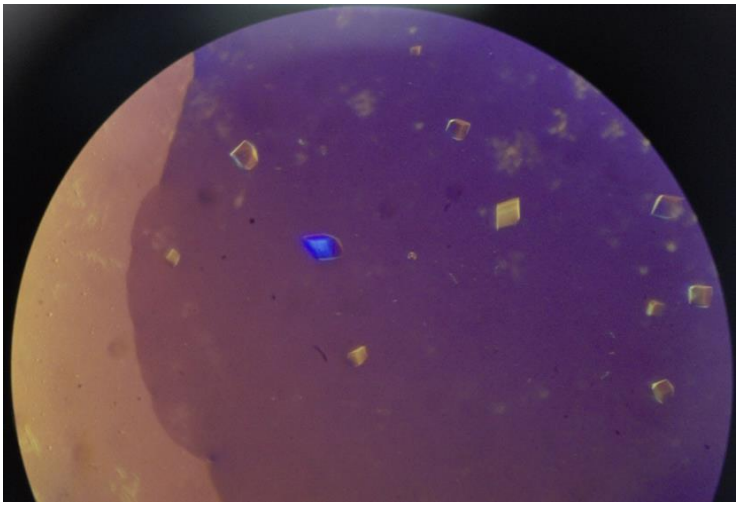

Figure 35 ***Apo state protein crystals****. Crystals seen in 24-Well Plate screen without the presence of any substrate (apo). Photo taken at 96x magnification.*

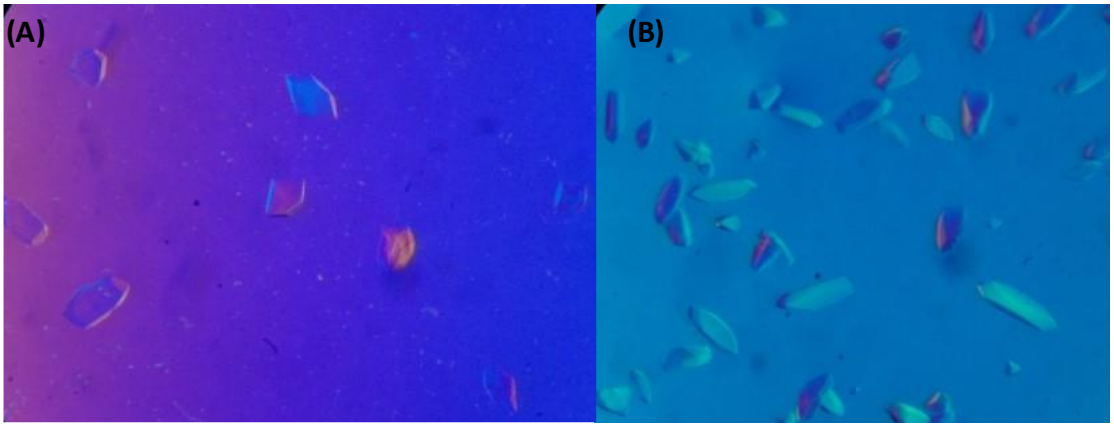

Figure 36 ***VC0430 crystallography condition optimisation****. (A) Crystals seen with 1 mM L-glutamine at ratio of 1:1 VC0430 to 2.4M SMDM. Many large crystals can be observed. (B) Crystals seen with 0.5 mM L-glutamate at a 1:1 ratio of VC0430 to 2.4M SMDM. An even greater number of even bigger crystals can be observed. Photos taken at 96x magnification.*

Chapter 4 Discussion

For the first time, we have been able to biochemically characterise the substrate binding of a TAXI-TRAP Transporter SBP. Using numerous substrate binding assays such as DSF and Intrinsic Tryptophan Fluorescence we have been able to quantify the binding affinity of VC0430 for its two key substrates: glutamate and glutamine with a Kd of 0.103 ± 0.051 µM and 18.525 ± 6.782 µM respectively. We have also shown that although VC0430 binds both glutamate and glutamine, there is a significant difference in affinity between them suggesting that possibly one of them is an

unintended secondary substrate. Furthermore, we also revealed that VC0430 can also bind the D enantiomer of glutamate and possibly of D-glutamine, but this could not be confirmed from our approach.

Using homology modelling in Phyre2 we were able to generate a structure of VC0430, which we could compare with the structure of TtGluBp to find key residues involved in binding of glutamate and glutamine. We were able to determine six binding clusters in which residues directly interact with the bound substrate in the structure, from these, four key residues in which their side chains directly interact with the ligand (Y45, Q93, E125 and M201) and one that does not apparently directly interact with the ligand but is conserved in TtGluBp and present in the binding site (Y200). We used site-directed mutagenesis to alanine to assess how important each residue was for binding L-glutamate/glutamine, revealing how mutating residues Y45 and Q93 to alanine drastically increased the Kd by more than 100 times that of wild type for both substrates and mutating Y200 to alanine completely prevented any detectable substrate binding. Such a major increase in Kd is indicative of how these residues are strong determinants for glutamate/glutamine ligand binding.

4.1.1. L-Glutamate and L-Glutamine Binding

We have shown how VC0430 can bind both L-glutamate and L-glutamine, but we have also shown that VC0430 binds L-glutamate with an affinity of close to 200 times greater than L-glutamine that falls in line with similar SBPs (Table 15). glutamate and glutamine are highly similar C5 dicarboxylates with the main difference being the presence of a 3 carbon-length acetoamide functional group in the sidechain instead of a 3 carbon-length carboxylic acid functional group. It has been observed how glutamate binding proteins can also bind glutamine but cannot transport it(41). It is possible that a similar result would be seen with VC0430 but further experimentation with the membrane component would be required. In the study on TtGluBp by Takahashi et al. the structure was solved with either L-glutamate or L-glutamine present but still showed many conserved residues that bind substrate(27). However, it still also gives a possible suggestion why VC0430 binds glutamine with a lower affinity than glutamate. At the carboxyl group of glutamate/glutamine the oxygens are directly coordinated by the backbone of Gly-142 and Thr-143 and the backbone of Gly-59 and Ser-60, however, only one of the side chain oxygens is coordinated by the backbone of Gly-30, Val-31, and Tyr-32 while the other displays no interaction. The structure of TtGluBp reveals a motif of a serine/threonine preceded by a glycine a total of four times in the sequence. Three of these motifs are seen in the binding site with two already seen to make interactions with the ligand (Figure 37). Of these three motifs in the

binding site, they are more conserved in VC0430 with the main difference being the presence Asp-157 instead of Ser-143 (BLOSUM62 score of 1) than the remaining motif not near the binding site containing Met-247 in VC0430 instead of Thr-251 in TTGluBp (BLOSUM62 score of -1). The remaining motif in the binding site (Gly-24, Ser-25, Gly-26, Ser-27) does not currently appear to interact with ligand but it is positioned in proximity to one of the sidechain carbonyls or acetoamide groups (Figure 37 (3)). As such, it is possible that due to the different bond resonance of the amine group the bond length would be different or the presence of the nitrogen prevents this hydrogen bond from forming. As these groups of residues near the binding site are conserved in VC0430 it is likely that they would exhibit the same substrate binding capabilities.

Table 15 ***Kd's of other SBPs****. A table showing the Kd for different substrates of other SBPs of the greater TRAP family.*

Protein Name	Original Organism	Kd (μM)	Ligand	Ref.
DctP-type TRAP SBPs				
TakP	*Rhodobacter sphaeroides*	0.26	α-ketoglutarate	(35)
SiaP	*Haemophilus influenzae*	0.12	Nea5Ac	(5)
TeaA	*Halomonas elongata*	0.19	Ectoine	(42)
TTT				
Bug27	*Bordetella pertussis*	0.36	Nictinamide	(16)
TAXI				
VC0430	*Vibrio cholerae*	0.10	L-Glutamate	

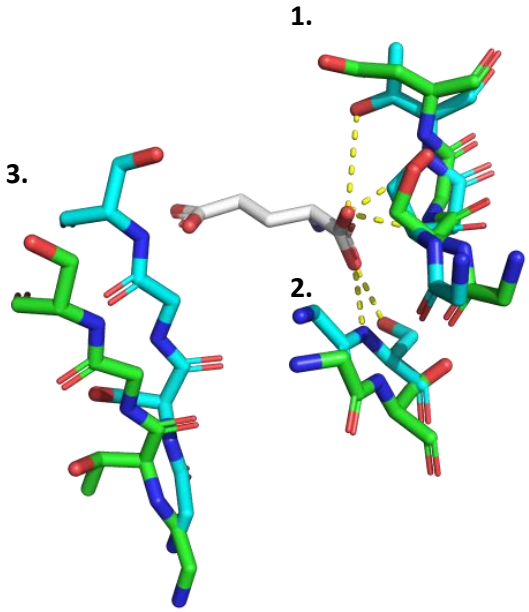

Figure 37 ***Serine in ligand binding****. Alignment of glycine and serine/threonine/aspartate motifs around bound substrate (white) for TTGluBp (cyan) and VC0430 (green) with hydrogen bonding depicted with yellow dashed lines. For motif 1 and 2 it can be observed how they interact with the carbonyl groups of bound substrates. In motif 3 no hydrogen bonds can be seen interacting with the carbonyl groups of the substrate sidechains despite their proximity to the residues. All the residues seen here are highly conserved and closely overlap with each other. TTGluBp PDB code: 1US4.*

4.1.2. Binding Differences Between the D and L Enantiomers of Glutamate and Glutamine

We have also shown that VC0430 can bind the D enantiomers of glutamate and possibly glutamine but with severely lower affinity or was not determinable (D-glutamine). While some D enantiomers of amino acids can be utilised by different organisms such as bacteria utilizing D-glutamic acid in their peptidoglycan cell wall(43,44) the vast majority of biological functions revolve around the L enantiomers of amino acids. In this case the main difference with the D enantiomer of glutamate/glutamine in the binding site would be that the N and carboxyl group would be switched to the opposite sites. In TtGluBp with L-glutamate/glutamine the amine group of the amino acid is coordinated by four residues (Tyr-32, Gln-78, Glu-111 and Thr-187) by four hydrogen bonds and the two carbonyl groups coordinated by another four residues (Gly-59, Ser-60, Gly-142 and Thr-143) by hydrogen bonds for a total of eight hydrogen bonds (Figure 38A). However, for the D enantiomers the carbonyl and amide groups would be in different environments which would alter the hydrogen bonds that would form. For the D enantiomer, only a total of three hydrogen bonds would be able to form (Figure 38B), one from Tyr-32 to one of the carbonyl groups and two from Thr-143 to the other carbonyl and amide group which would result in a major decrease in binding activity which was observed. Regarding, the potential binding observed for D-glutamine, we showed how VC0430 already weakly binds L-glutamine so fewer hydrogen bonds forming, particularly as it is likely that L-glutamine is only able to bind because

of the interactions of the amine and carbonyl groups not in the sidechain, would result in an even lower binding affinity or possibly not bind at all. Based on the similarity and conservation of residues in TTGluBp and VC0430, this binding character would likely also apply to VC0430. However, this is all speculation based on a modified pre-existing structure, to confirm if this binding character was correct VC0430 would have to be crystallised and solved in the presence of D-glutamate and glutamine.

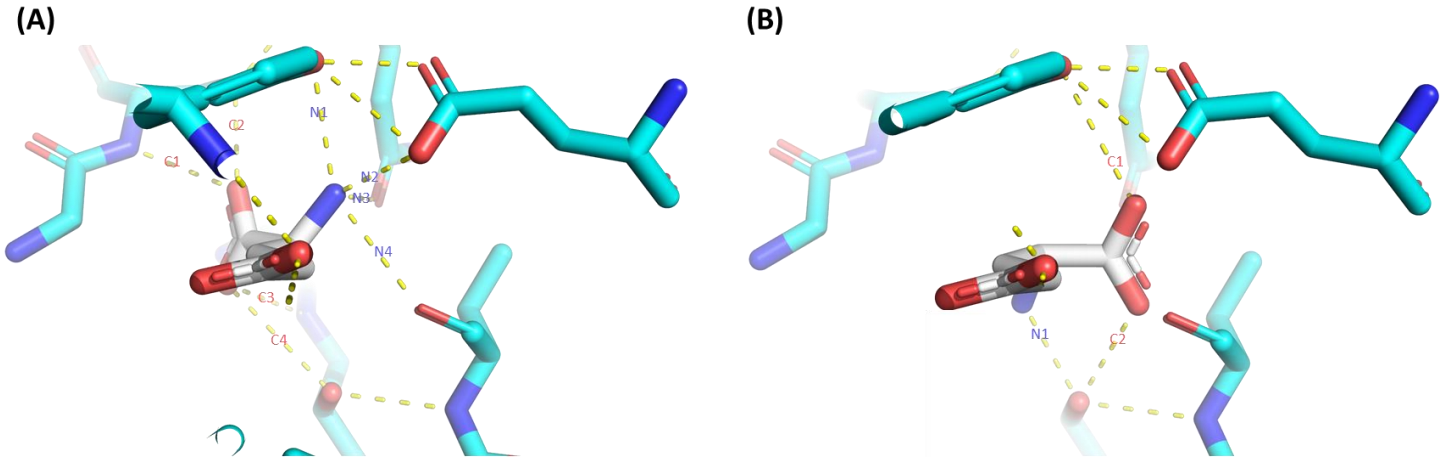

Figure 38 ***D and L enantiomer binding****. (A). A model of TTGluBp binding L-glutamate/glutamine (white) with hydrogen bonds represented by the yellow dashed line. Four residues form four hydrogen bonds with the non-sidechain amine group (N1-4). Four residues form another four hydrogen bonds with the two remaining non-sidechain carbonyl groups (C1-4) of the substrate for a total of eight hydrogen bonds. (B). A modified version of (A) to represent bound D-glutamate/glutamine (white) with hydrogen bonds represented by a yellow dashed line. One residue forms a hydrogen bond with the non-sidechain amine group (N1) and one of the non-sidechain carbonyl groups (C2). One other residue also forms one hydrogen bond with the remaining non-sidechain carbonyl group (C1) for a total of three hydrogen bonds.*

4.1.3. Glutamate Binding in the SBPs of Other TRAP Transporter Families

The only known structure of a TAXI-TRAP SBP with glutamate or glutamine bound is TtGluB but the structure of a similar family of transporters (TTT) has been solved with glutamate bound, known as BugE(17). We aligned the structure of VC0430 onto BugE which yielded minimal alignment in the binding site (Figure 39) but revealed similarities in the general amino acid composition. One major similarity is the positioning of two sidechain aromatic rings above and below parallel to the substrate, but with a phenylalanine instead of a tyrosine that was seen in

VC0430 and TTGluBp. Interestingly, using PyMol's measuring tool we found that the distance between the zeta carbon of each ring was 8.0 Å which is highly similar to the measured distance between the zeta carbon of the aromatic residues in VC0430 and TTGluBp (7.4 Å and 8.6 Å respectively). A pair of aromatic residues is likely key for binding amino acids due to their aliphatic carbon chain, a pair of aromatic rings positioned above and below the aliphatic region likely allows specific non-polar interactions and Van Der Waals forces that enables the amino acid to be held in place(45). Furthermore, in a DctP-type TRAP SBP that binds pyroglutamate, another pair of aromatic rings 8.3 Å apart can be seen, although this time one of the residues is a tryptophan(46). It is likely that due to the increased aliphatic region of pyroglutamate by the additional aliphatic ring that a larger surface area is required (given by the additional ring in tryptophan) to allow for more Van Der Waals forces as seen with cyclic sugars by N. K. Vyas et al.(45). BugE also forms hydrogen bonds with the more polar carboxyl groups from hydroxyl groups present in the sidechain of the residue. Interestingly, in VC0430 and TTGluBp there is more interactions with substrate from carboxyl groups as opposed to a key dependence on hydroxyl groups that are seen in BugE. Additionally, while the specific amino acid composition of the binding site of VC0430 and TTGluBp is quite diverse, in BugE the majority if residue sidechains that directly interact with the substrate are serine's (Figure 40). Hydrogen bonding to the amine group can also be seen in BugE (Figure 40) but with half the number of residues that bind to it in TTGluBp, suggesting that perhaps only one or two specific hydrogen bonds are required to effectively coordinate the amine group which would correlate with what we saw with VC0430 in residue Q93. Despite the very minor sequence similarity in the alignment, it is clear than for these TRAP family transporters the key to binding glutamate/glutamine relies on non-polar interactions from aromatic residues and hydrogen bonds between carbonyl groups.

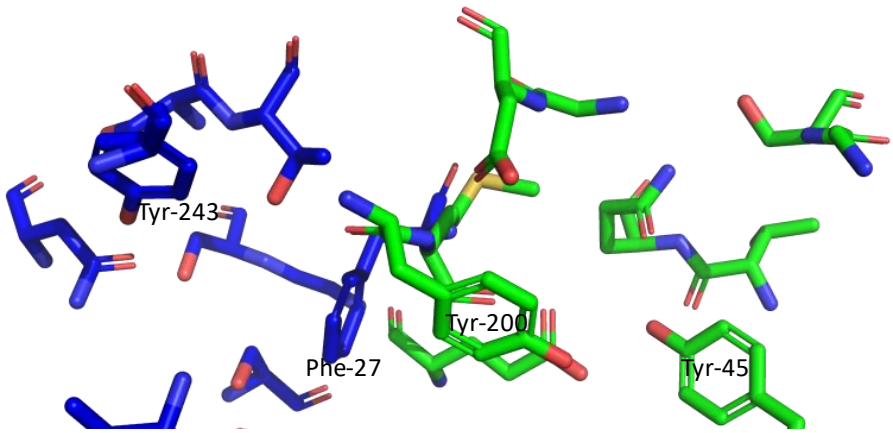

Figure 39 ***BugE VC0430 binding site alignment****. Structural alignment of the binding site of VC0430 (green) and BugE (Blue). A structural alignment of VC0430 and BugE yielded very limited success but did reveal similarities in the general amino acid composition of the binding site, particularly of note is the pair of aromatic residues (tyrosine's and phenylalanine's, labelled) in each binding site.*

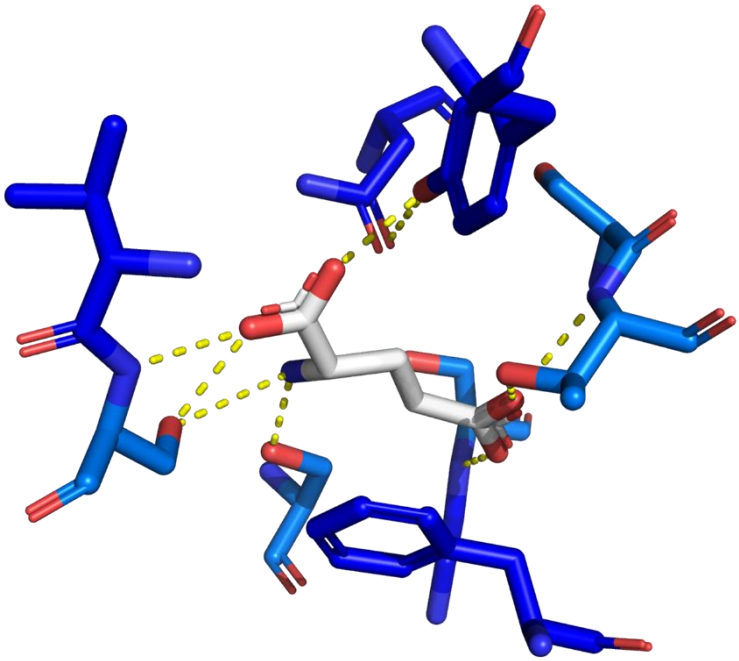

Figure 40 ***Glutamate binding in the BugE binding site****. Binding site of BugE with bound glutamate (white) with hydrogen bonds depicted as yellow dashed lines. The binding site of BugE shows how much of glutamate is coordinated by hydrogen bonds from hydroxyl groups of serine and threonine sidechains (coloured in marine blue). A fewer number of hydrogen bonds to the amine group of glutamate is observed.*

4.1.4. Mutagenesis and Tryptophan fluorescence

Of five total residues in VC0430 mutated into alanine in this project, Y45A, Q93A and Y200A had the biggest impact on the affinity of VC0430. The Y45A mutation resulted in a major increase in Kd by approximately 150 times that of wild type. In the binding site of VC0430 Y45 likely has two major roles in ligand binding based on the TtGluBp model: the hydroxyl group of Tyr-45 directly forms hydrogen bonds with the amine group of the bound glutamate and the aromatic surface likely allows the formation of non-polar interactions in conjunction with Tyr-200 to coordinate the

bound substrate, as described prior and seen in similar proteins (Figure 26A and 41A)(47,48). As such, it is unsurprising why mutating this residue to alanine caused such a major reduction in affinity, as the hydrogen bond to the amine group would not be able to form and altering the aromatic ring would greatly disrupt the non-polar interactions to substrate. To further test the importance of the Tyr-45 amine hydrogen bond the tyrosine could be mutated into phenylalanine to potentially maintain a similar surface area for non-polar interactions. The Q93A mutation on the other hand was more surprising as the model reveals the formation of one hydrogen bond to the amine group of the ligand despite an approximate 700 times greater Kd than wild type. The mutation to alanine would prevent the formation of this hydrogen bond, so it is possible that for VC0430 to bind its substrate at the amine group that this hydrogen bond is crucial. Although Tyr-200 does not seem to form any hydrogen bonds with the ligand it would likely be required in tandem with Tyr-45 to coordinate the substrate with non-polar interactions. A mutation to alanine would significantly increase the distance between the substrate and residue (Figure 41) which would put the alanine out of Van Der Waals forming range and therefore prevent the non-polar interactions to coordinate substrate. This would be a likely explanation of why this mutation completely prevented substrate binding and highlights the importance of these non-polar interactions for binding substrate in VC0430. However, to further confirm the importance of these non-polar interactions, both tyrosine's could be mutated to phenylalanine to see how it would impact substrate binding.

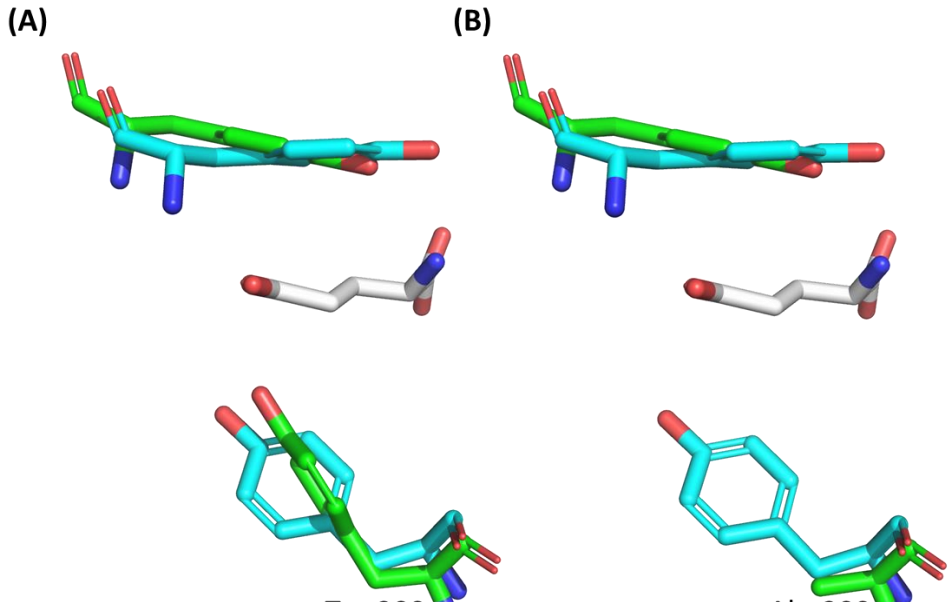

Figure 41 ***A detailed look at the Y200A mutation in VC0430****. (A). The tyrosine's of TTGluBp in the binding site (cyan) aligned with the tyrosine's in the predicted binding site of VC0430 (green) around bound substrate (grey). (B). The same alignment as (A) but with Tyr-200 mutated to Ala-200 (labelled). Mutating Tyr-200 to alanine significantly increases the distance between the residue and the bound substrate, out of Van Der Waals distance which would greatly affect binding.*

The remaining mutants (E125 and M201) resulted in a minor decrease in affinity of 2-3 times compared to wild type. The E125A mutation would disrupt two hydrogen bonds from the carboxylate group of the residue to the amine group of the ligand (Figure 26B) but do not affect the Kd much, highlighting the importance of Q93 in hydrogen bonding to the amine group of the substrate. Mutating Met-201 to alanine would only disrupt one hydrogen bond from the carbonyl group to the substrate (Figure 26D) and alter the carbon-chain length but the functional group responsible for forming the hydrogen group would still be present.

4.1.5. Increase In Tryptophan Fluorescence Enhancement

For all the mutants that showed fluorescence activity we observed that many of them resulted in a greater fluorescence enhancement as compared to wild type. The greatest enhancement of WT seen was close to 8 % but all other active mutants saw an enhancement of at least 12 %. Upon inspection of the binding site, it is possible that replacement of all of the binding residues with alanine would result in in a smaller carbon chain length in all cases so Trp-96 might become more buried as the conformation of VC0430 changes upon binding, resulting in a more extreme change in environment which could cause a bigger enhancement(36).

4.2. Significance of Glutamate and Glutamine in *Vibrio cholerae*

4.2.1. The Role of Glutamate in Osmoadaptation

V. cholerae is a gram-negative halophile that resides in an estuarine environment. These environments are often subject to fluctuations in ionic strength making it very challenging for bacteria to survive, however *V. cholerae* has adapted mechanisms to maintain its osmotic pressure in these more harsh environments(49). In their study of glutamate uptake levels in *V. Cholerae* by Munro et al. they found that increased osmotic pressure of the cell media resulted in a greater uptake of glutamate(50) and thus hinting in a potential role of glutamate in surviving these conditions. This idea was later expanded upon by another study on which they found how the knockout of the gene ectA, important for producing ectoine in *V. Cholerae*, would prevent the survival and growth of *V. cholerae* at higher saline levels(49). However, re-introducing glutamate to these cells significantly increased growth as glutamate is a

precursor of ectoine(49,51). Ectoine is known as a compatible solute with protective functions of protein in part due to its high affinity for water, explained by the "preferential exclusion model": The solutes are excluded from the immediate hydration shell of a protein because of unfavourable protein surface interactions resulting in hydration of the protein but without direct contact of the solute to the protein so the catalytic activity remains unchanged(52). As such, it stands to reason that for *V. cholerae* to survive in high saline conditions it requires glutamate and VC0430 may be a key part of a membrane transporter to import glutamate into the cell for conversion to ectoine. Further experiments should be done in *V. cholerae* with the VC0430 gene knocked out to see how this would affect growth in these higher saline conditions.

4.2.2. Speculation of the Role of Glutamine in *Vibrio cholerae*

Currently, there is no literature that reveals the role of glutamine in *V. cholerae* despite the use of it as a general carbon source. Furthermore, an analysis of a highly saline environment (sea water) in "Marine Organic Chemistry: Evolution, Composition, Interactions and Chemistry of Organic Matter in Seawater" by R. Dawson and G. Liebezeit revealed that with current methods there is very low levels of free-floating glutamine as compared to glutamate and others(53). Therefore, on the assumption that seawater would be like a *V. cholerae* environment it is possible that glutamine is present in such low amounts that it would be disadvantageous to specifically import it. Based on the data we have collected during this project, I believe that VC0430's primary function is to bind glutamate to take in into the cell to make ectoine and that it only binds glutamine as well because of how similar its structure is compared to glutamate. It has been shown in humans how important glutamate is for things like linking carbohydrate and amino acid metabolism and as such a glutaminase exists that is able to convert glutamine to glutamate(54). It is possible that if *V. cholerae* needs large quantities of glutamate to make ectoine then it may also contain a system for converting other compounds such as glutamine to glutamate, but more experiments would be needed to confirm this. If this is the case, then at some point during evolution it may have been no longer beneficial to achieve an even more specific binding site for glutamate as being able to bind glutamine could have still been advantageous if it could be converted to glutamate. However, as described by Jacobs et al.(41) just because the SBP binds glutamine does not necessarily mean that it will be able to transport it, more experimentation would be needed to confirm if this was the case with VC0430.

4.3. VC0430 as a Potential Drug Target for Treating Vibrio Cholerae

Although cholera is eradicated in most of the world, it is still prevalent in many low income countries with an estimated 1.3 to 4 million reported cases causing between 21,000 to 143,000 deaths per year(55). Therefore, cholera is still a major risk to many people with outbreaks frequently correlated to natural disasters such as monsoons(56). Due to the synthesis of ectoine aiding survival in high saline environments, it has also been suggested that ectoine may play a key role in survival of *V. Cholerae* in the high osmolarity in the intestine(49). As such the dependence of VC0430 in glutamate to survive in these conditions makes VC0430 an ideal drug target. If VC0430 can be inhibited, then it would prevent *V. Cholerae* from importing glutamate and therefore produce ectoine to survive. Although VC0430 is only a small component of a bigger membrane transporter system, these systems typically rely on an SBP to bind the substrate with high specificity and affinity and move it to the translocation machinery at the cell membrane(7). Therefore, inhibiting the SBP would entirely prevent the uptake of the corresponding substrate. However, this would be only effective if the VC0430 transport system is the only transport that allows glutamate uptake which could be determined by performing growth assays of V. cholerae in glutamate/glutamine minimal media with VC0430 knockout strains.

Conclusion

The work done in this project aimed to characterize the binding and binding site of the TAXI-TRAP SBP VC0430 for glutamate and glutamine with a combination of *In silico* and *in vitro* methods. We have shown how VC0430 is a highly specific binding protein with an affinity for L-glutamine (Kd: 18.53 ± 6.78 µM) but an even higher affinity for L-glutamate (Kd: 0.10 ± 0.051 µM). We have also shown that VC0430 shows some stereoselectivity in substrate as it was not able to bind D-glutamine but could bind D-glutamate with a considerably lower affinity (Kd: 24.51 ± 10.15 µM) suggesting that it is not the intended substrate. From 12 binding site residues we were able to assess the selectivity determinants by alanine mutagenesis of five of them: Y45, Q93, E125, Y200 and M201. We observed that mutations of Y45 (Glu Kd: 15.82 ± 1.58 µM, Gln Kd: 8665.33 ± 2603.74 µM) and Q93 (Glu Kd: 74.93 ± 17.78 µM, Gln Kd: N.D.) significantly reduced binding affinity while Y200 completely prevented binding, suggesting that these

residues are key selectivity determinants in VC0430. The remaining mutations in residues E125 (Glu Kd: 0.27 ± 0.11 µM, Gln Kd: 36.75 ± 13.9 µM) and M201 (Glu Kd: 0.33 ± 0.1 µM, Gln Kd: 48.64 ± 15.69 µM) resulted in a minor decrease in binding affinity, suggesting that that these residues are likely not key selectivity determinants in VC0430.

One of the major limitations of this work is that binding site predictions have been heavily based of a different but similar protein TTGluBP due to a current lack of any structures of VC0430. As such, further work will include solving the structure of VC0430 from crystals we have grown with no substrate, L-glutamate and L-glutamine by X-ray diffraction to confirm ligand binding as we have predicted and to expand the repertoire of current TAXI-TRAP Transporter structures. Additional experiments will also take place to probe the importance of the remaining seven residues in the binding site (G43, V44, G74, S75, V92, G156 and D157).

1. KABACK HR. CHAPTER 6 - Active Transport: Membrane Vesicles, Bioenergetics, Molecules, and Mechanisms. In: Krulwich TABT-BE, editor. Academic Press; 1990. p. 151–202. Available from: https://www.sciencedirect.com/science/article/pii/B9780123072122500107

2. Wilkens S. Structure and mechanism of ABC transporters. F1000Prime Rep. 2015;7:14.

3. Locher KP. Review. Structure and mechanism of ATP-binding cassette transporters. Philos Trans R Soc London Ser B, Biol Sci. 2009 Jan;364(1514):239–45.

4. Neu HC, Heppel LA. The Release of Enzymes from *Escherichia coli* by Osmotic Shock and during the Formation of Spheroplasts. J Biol Chem [Internet]. 1965;240(9):3685–92. Available from: https://www.sciencedirect.com/science/article/pii/S0021925818972005

5. Müller A, Severi E, Mulligan C, Watts AG, Kelly DJ, Wilson KS, et al. Conservation of Structure and Mechanism in Primary and Secondary Transporters Exemplified by SiaP, a Sialic Acid Binding Virulence Factor from Haemophilus influenzae*. J Biol Chem [Internet]. 2006 Aug 4;281(31):22212–22. Available from: https://doi.org/10.1074/jbc.M603463200

6. Tanaka KJ, Song S, Mason K, Pinkett HW. Selective substrate uptake: The role of ATP-binding cassette (ABC) importers in pathogenesis. Biochim Biophys acta Biomembr. 2018 Apr;1860(4):868–77.

7. Mulligan C, Fischer M, Thomas GH. Tripartite ATP-independent periplasmic (TRAP) transporters in bacteria and archaea. FEMS Microbiol Rev [Internet]. 2011 Jan 1;35(1):68–86. Available from: https://doi.org/10.1111/j.1574-6976.2010.00236.x

8. Kelly DJ, Thomas GH. The tripartite ATP-independent periplasmic (TRAP) transporters of bacteria and archaea. FEMS Microbiol Rev [Internet]. 2001 Aug 1;25(4):405–24. Available from: https://doi.org/10.1111/j.1574-6976.2001.tb00584.x

9. Forward JA, Behrendt MC, Wyborn NR, Cross R, Kelly DJ. TRAP transporters: a new family of periplasmic solute transport systems encoded by the dctPQM genes of Rhodobacter capsulatus and by homologs in diverse gram-negative bacteria. J Bacteriol. 1997 Sep;179(17):5482–93.

10. Rosa LT, Dix SR, Rafferty JB, Kelly DJ. Structural basis for high-affinity adipate binding to AdpC (RPA4515), an orphan periplasmic-binding protein from the tripartite tricarboxylate transporter (TTT) family in Rhodopseudomonas palustris. FEBS J [Internet]. 2017 Dec 1;284(24):4262–77. Available from: https://doi.org/10.1111/febs.14304

11. Peter MF, Gebhardt C, Glaenzer J, Schneberger N, de Boer M, Thomas GH, et al. Triggering Closure of a Sialic Acid TRAP Transporter Substrate Binding Protein through Binding of Natural or Artificial Substrates. J Mol Biol. 2021 Feb;433(3):166756.

12. Rosa LT, Bianconi ME, Thomas GH, Kelly DJ. Tripartite ATP-Independent Periplasmic (TRAP) Transporters and Tripartite Tricarboxylate Transporters (TTT): From Uptake to Pathogenicity. Front Cell Infect Microbiol. 2018;8:33.

13. Mulligan C, Geertsma ER, Severi E, Kelly DJ, Poolman B, Thomas GH. The substrate-binding protein imposes directionality on an electrochemical sodium gradient-driven TRAP transporter. Proc Natl Acad Sci [Internet]. 2009 Feb 10;106(6):1778–83. Available from: https://doi.org/10.1073/pnas.0809979106

14. Sweet GD, Somers JM, Kay WW. Purification and properties of a citrate-binding transport component, the C protein of Salmonella typhimurium. Can J Biochem. 1979 Jun;57(6):710–5.

15. Winnen B, Hvorup RN, Saier MH. The tripartite tricarboxylate transporter (TTT) family. Res Microbiol [Internet]. 2003;154(7):457–65. Available from: https://www.sciencedirect.com/science/article/pii/S0923250803001268

16. Herrou J, Bompard C, Antoine R, Leroy A, Rucktooa P, Hot D, et al. Structure–based Mechanism of Ligand Binding for Periplasmic Solute-binding Protein of the Bug Family. J Mol Biol [Internet]. 2007;373(4):954–64.

Available from: https://www.sciencedirect.com/science/article/pii/S0022283607010637

17. Huvent I, Belrhali H, Antoine R, Bompard C, Locht C, Jacob-Dubuisson F, et al. Structural analysis of {\it Bordetella pertussis} BugE solute receptor in a bound conformation. Acta Crystallogr Sect D [Internet]. 2006 Nov;62(11):1375–81. Available from: https://doi.org/10.1107/S0907444906032653

18. Huvent I, Belrhali H, Antoine R, Bompard C, Locht C, Jacob-Dubuisson F, et al. Crystal structure of Bordetella pertussis BugD solute receptor unveils the basis of ligand binding in a new family of periplasmic binding proteins. J Mol Biol. 2006 Mar;356(4):1014–26.

19. Rosa LT, Dix SR, Rafferty JB, Kelly DJ. A New Mechanism for High-Affinity Uptake of C4-Dicarboxylates in Bacteria Revealed by the Structure of Rhodopseudomonas palustris MatC (RPA3494), a Periplasmic Binding Protein of the Tripartite Tricarboxylate Transporter (TTT) Family. J Mol Biol. 2019 Jan;431(2):351–67.

20. Mulligan C, Leech AP, Kelly DJ, Thomas GH. The membrane proteins SiaQ and SiaM form an essential stoichiometric complex in the sialic acid tripartite ATP-independent periplasmic (TRAP) transporter SiaPQM (VC1777-1779) from Vibrio cholerae. J Biol Chem. 2012 Jan;287(5):3598–608.

21. Fischer M, Zhang QY, Hubbard RE, Thomas GH. Caught in a TRAP: substrate-binding proteins in secondary transport. Trends Microbiol [Internet]. 2010;18(10):471–8. Available from: https://www.sciencedirect.com/science/article/pii/S0966842X10001113

22. Fischer M, Hopkins AP, Severi E, Hawkhead J, Bawdon D, Watts AG, et al. Tripartite ATP-independent Periplasmic (TRAP) Transporters Use an Arginine-mediated Selectivity Filter for High Affinity Substrate Binding *. J Biol Chem [Internet]. 2015 Nov 6;290(45):27113–23. Available from: https://doi.org/10.1074/jbc.M115.656603

23. Allen S, Zaleski A, Johnston JW, Gibson BW, Apicella MA. Novel sialic acid transporter of Haemophilus influenzae. Infect Immun. 2005 Sep;73(9):5291–300.

24. Mayfield JE, Bricker BJ, Godfrey H, Crosby RM, Knight DJ, Hailing SM, et al. The cloning, expression, and nucleotide sequence of a gene coding for an immunogenic Brucella abortus protein. Gene [Internet]. 1988;63(1):1–9. Available from: https://www.sciencedirect.com/science/article/pii/0378111988905409

25. Berntsson RP-A, Smits SHJ, Schmitt L, Slotboom D-J, Poolman B. A structural classification of substrate-binding proteins. FEBS Lett [Internet]. 2010;584(12):2606–17. Available from: https://www.sciencedirect.com/science/article/pii/S0014579310003273

26. Rabus R, Jack DL, Kelly DJ, Saier MHJ. TRAP transporters: an ancient family of extracytoplasmic solute-receptor-dependent secondary active transporters. Microbiology. 1999 Dec;145 (Pt 1:3431–45.

27. Takahashi H, Inagaki E, Kuroishi C, Tahirov TH. Structure of the Thermus thermophilus putative periplasmic glutamate/glutamine-binding protein. Acta Crystallogr Sect D [Internet]. 2004 Oct 1;60(10):1846–54. Available from: https://doi.org/10.1107/S0907444904019420

28. Ayala-del-Río HL, Chain PS, Grzymski JJ, Ponder MA, Ivanova N, Bergholz PW, et al. The genome sequence of Psychrobacter arcticus 273-4, a psychroactive Siberian permafrost bacterium, reveals mechanisms for adaptation to low-temperature growth. Appl Environ Microbiol. 2010 Apr;76(7):2304–12.

29. Sanz D, García JL, Díaz E. Expanding the current knowledge and biotechnological applications of the oxygen-independent ortho-phthalate degradation pathway. Environ Microbiol [Internet]. 2020 Aug 1;22(8):3478–93. Available from: https://doi.org/10.1111/1462-2920.15119

30. Deka RK, Brautigam CA, Goldberg M, Schuck P, Tomchick DR, Norgard M V. Structural, Bioinformatic, and In Vivo Analyses of Two Treponema pallidum Lipoproteins Reveal a Unique TRAP Transporter. J Mol Biol [Internet]. 2012;416(5):678–96. Available from: https://www.sciencedirect.com/science/article/pii/S0022283612000691

31. Brautigam CA, Deka RK, Schuck P, Tomchick DR, Norgard M V. Structural and Thermodynamic Characterization of the Interaction between Two Periplasmic Treponema pallidum Lipoproteins that are Components of a TPR-Protein-Associated TRAP Transporter (TPAT). J Mol Biol [Internet]. 2012;420(1):70–86.

Available from: https://www.sciencedirect.com/science/article/pii/S002228361200304X

32. Vedadi M, Niesen FH, Allali-Hassani A, Fedorov OY, Finerty PJJ, Wasney GA, et al. Chemical screening methods to identify ligands that promote protein stability, protein crystallization, and structure determination. Proc Natl Acad Sci U S A. 2006 Oct;103(43):15835–40.

33. Helling RB. Pathway choice in glutamate synthesis in *Escherichia coli*. J Bacteriol. 1998 Sep;180(17):4571–5.

34. Niesen FH, Berglund H, Vedadi M. The use of differential scanning fluorimetry to detect ligand interactions that promote protein stability. Nat Protoc [Internet]. 2007;2(9):2212–21. Available from: https://doi.org/10.1038/nprot.2007.321

35. Gonin S, Arnoux P, Pierru B, Lavergne J, Alonso B, Sabaty M, et al. Crystal structures of an Extracytoplasmic Solute Receptor from a TRAP transporter in its open and closed forms reveal a helix-swapped dimer requiring a cation for α-keto acid binding. BMC Struct Biol [Internet]. 2007;7(1):11. Available from: https://doi.org/10.1186/1472-6807-7-11

36. Ghisaidoobe ABT, Chung SJ. Intrinsic tryptophan fluorescence in the detection and analysis of proteins: a focus on Förster resonance energy transfer techniques. Int J Mol Sci. 2014 Dec;15(12):22518–38.

37. Yang H, Xiao X, Zhao X, Wu Y. Intrinsic fluorescence spectra of tryptophan, tyrosine and phenyloalanine. In: ProcSPIE [Internet]. 2017. p. 102554M. Available from: https://doi.org/10.1117/12.2268397

38. KAPUST RB, WAUGH DS. *Escherichia coli* maltose-binding protein is uncommonly effective at promoting the solubility of polypeptides to which it is fused. Protein Sci [Internet]. 1999/08/01. 1999;8(8):1668–74. Available from: https://www.cambridge.org/core/article/escherichia-coli-maltosebinding-protein-is-uncommonly-effective-at-promoting-the-solubility-of-polypeptides-to-which-it-is-fused/142C9BFF119AD85641035798530AB550

39. Kapust RB, Tözsér J, Fox JD, Anderson DE, Cherry S, Copeland TD, et al. Tobacco etch virus protease: mechanism of autolysis and rational design of stable mutants with wild-type catalytic proficiency. Protein Eng Des Sel [Internet]. 2001 Dec 1;14(12):993–1000. Available from: https://doi.org/10.1093/protein/14.12.993

40. de Boer M, Gouridis G, Vietrov R, Begg SL, Schuurman-Wolters GK, Husada F, et al. Conformational and dynamic plasticity in substrate-binding proteins underlies selective transport in ABC importers. Aldrich R, Chanda B, Chanda B, Goldschen-Ohm MP, editors. Elife [Internet]. 2019;8:e44652. Available from: https://doi.org/10.7554/eLife.44652

41. Jacobs MH, Driessen AJ, Konings WN. Characterization of a binding protein-dependent glutamate transport system of Rhodobacter sphaeroides. J Bacteriol. 1995 Apr;177(7):1812–6.

42. Kuhlmann SI, Terwisscha van Scheltinga AC, Bienert R, Kunte H-J, Ziegler C. 1.55 Å Structure of the Ectoine Binding Protein TeaA of the Osmoregulated TRAP-Transporter TeaABC from Halomonas elongata. Biochemistry [Internet]. 2008 Sep 9;47(36):9475–85. Available from: https://doi.org/10.1021/bi8006719

43. Hancock R. The amino acid composition of the protein and cell wall of Staphylococcus aureus. Biochim Biophys Acta [Internet]. 1960;37(1):42–6. Available from: https://www.sciencedirect.com/science/article/pii/0006300260900767

44. Park JT, Strominger JL. Mode of Action of Penicillin . Science (80-) [Internet]. 1957 Jan 18;125(3238):99–101. Available from: https://doi.org/10.1126/science.125.3238.99

45. Vyas NK, Vyas MN, Quiocho FA. Sugar and signal-transducer binding sites of the *Escherichia coli* galactose chemoreceptor protein. Science. 1988 Dec;242(4883):1290–5.

46. Rucktooa P, Antoine R, Herrou J, Huvent I, Locht C, Jacob-Dubuisson F, et al. Crystal Structures of two Bordetella pertussis Periplasmic Receptors Contribute to Defining a Novel Pyroglutamic Acid Binding DctP Subfamily. J Mol Biol [Internet]. 2007;370(1):93–106. Available from: https://www.sciencedirect.com/science/article/pii/S0022283607005396

47. P.-A. BR, H. TA-MW, Bert P, Dirk-Jan S. Importance of a Hydrophobic Pocket for Peptide Binding in Lactococcal

OppA. J Bacteriol [Internet]. 2011 Aug 15;193(16):4254–6. Available from: https://doi.org/10.1128/JB.00447-11

48. Sun Y-J, Rose J, Wang B-C, Hsiao C-D. The structure of glutamine-binding protein complexed with glutamine at 1.94 Å resolution: comparisons with other amino acid binding proteins11Edited by R. Huber. J Mol Biol [Internet]. 1998;278(1):219–29. Available from: https://www.sciencedirect.com/science/article/pii/S0022283698916758

49. Pflughoeft KJ, Kierek K, Watnick PI. Role of Ectoine in Vibrio cholerae Osmoadaptation. Appl Environ Microbiol [Internet]. 2003 Oct;69(10):5919–27. Available from: https://journals.asm.org/doi/10.1128/AEM.69.10.5919-5927.2003

50. Munro PM, Gauthier MJ. Uptake of glutamate by Vibrio cholerae in media of low and high osmolarity, and in seawater. Lett Appl Microbiol [Internet]. 1994 Apr 1;18(4):197–9. Available from: https://doi.org/10.1111/j.1472-765X.1994.tb00845.x

51. Ono H, Sawada K, Khunajakr N, Tao T, Yamamoto M, Hiramoto M, et al. Characterization of biosynthetic enzymes for ectoine as a compatible solute in a moderately halophilic eubacterium, Halomonas elongata. J Bacteriol. 1999 Jan;181(1):91–9.

52. Graf R, Anzali S, Buenger J, Pfluecker F, Driller H. The multifunctional role of ectoine as a natural cell protectant. Clin Dermatol. 2008;26(4):326–33.

53. Dawson R, Liebezeit G. Chapter 15 The Analytical Methods for the Characterisation of Organics in Seawater. In: Duursma EK, Dawson RBT-EOS, editors. Marine Organic Chemistry [Internet]. Elsevier; 1981. p. 445–96. Available from: https://www.sciencedirect.com/science/article/pii/S0422989408703374

54. Schousboe A, Scafidi S, Bak LK, Waagepetersen HS, McKenna MC. Glutamate metabolism in the brain focusing on astrocytes. Adv Neurobiol. 2014;11:13–30.

55. Ali M, Nelson AR, Lopez AL, Sack DA. Updated global burden of cholera in endemic countries. PLoS Negl Trop Dis. 2015;9(6):e0003832.

56. Ali M, Emch M, Donnay JP, Yunus M, Sack RB. The spatial epidemiology of cholera in an endemic area of Bangladesh. Soc Sci Med. 2002 Sep;55(6):1015–24.